freezing behavior was observed for a 5-min period, during which no tone CS was presented. Secondly, we measured long-term memory as follows. Two hours later, the rats were again introduced into the conditioning chamber and freezing behavior was measured for a 5-min period, during which no tone CS was presented. Then, the rats were observed for another 5-min period, during which tone CS was presented. Tone CS-induced freezing behavior is dependent on the amygdala, while no-tone-CS-induced freezing behavior is dependent on the hippocampus [12].

Freezing behavior was evaluated in terms of total freezing time during a 5-min stay in the conditioning chamber and expressed as % freezing time. Freezing behavior was defined as cessation of all but respiratory movement.

2.3. Immunohistochemical study

At 2 h after the footshock, the rats were placed in the conditioning chamber and freezing behavior was measured without and with tone CS. Immediately after the series of measurements was over, the rats were sacrificed by decapitation. The brain was removed within 90 s and rapidly frozen in dry ice-isopentane, and kept at −70 °C until processing as was described in our previous paper [14]. Our previous study demonstrated that CREB phosphorylation occurs during as early as 1 h after the conditioning and lasted over 24 h [14], so that we considered that observation at 2 h may represent early process of long-term memory formation.

According to Paxinos and Watson's brain map [23], 10-μm coronal sections throughout the hippocampal formation (2.9 mm posterior to bregma suture) were cut using a cryostat (CM1850, Leica, Tokyo, Japan) and then attached to 3-aminopropyltriethoxysilane-coated glass slides (S8441, Matsunami Glass, Osaka, Japan). Sections were fixed in 4% paraformaldehyde in 0.1 M phosphate buffer, pH 7.4 for 10 min, and washed twice in 0.01 M phosphate-buffered saline, pH 7.4 for 10 min each. The sections were dehydrated in three changes of 70, 95, and 100% ethanol and re-hydrated in the reverse order of ethanol. The method was shown in a preliminary experiment to be effective in decreasing background staining. The sections were stored in −20 °C cryoprotectant (25% ethylene glycol, 25% glycerine in 0.05 M phosphate buffer) until immunostaining. The sections were incubated in 3% H_2O_2 in phosphate-buffered saline for 10 min to block endogenous peroxidase activity, and then in 10% normal horse serum in Tris-buffered saline, pH 7.4 (TBS) for 30 min to block nonspecific staining.

Thereafter, the sections were treated with either a 1:1500 dilution of anti-pCREB antibody (New England Biolabs, Beverly, MA, USA) which is a specific marker of CREB phosphorylated at Ser133, or anti-CREB antibody (1:1200 dilution) which binds to both the phosphorylated and unphosphorylated form of CREB in TBS containing 10% horse serum at 4 °C for 48 h. Then, the immunoreactive specificity was confirmed by omitting the primary antibody, which resulted in no stained cell in the hippocampus.

The sections were then incubated in biotinylated anti-rabbit IgG (Vector, Burlingame, CA, USA) diluted at 1:200 in TBS containing 10% normal horse serum for 1 h, washed in three changes of TBS containing 0.3% Tween 20 for 7 min each, followed by incubation with avidin-biotinylated horseradish peroxidase complex (Vectastain Elite ABC kit, Vector) in TBS for 1 h. Peroxidase reaction was performed using DAB Peroxidase Substrate Tablet Set (Sigma, St. Louis, MO, USA) in 1% nickel ammonium sulfate. Sections were dehydrated with ethanol, cleared with xylene, and cover-slipped with Histomount (Zymed, San Francisco, CA, USA).

Microscopic images of randomized sections were captured into a computer with a highly sensitive CCD camera (DP-50, Olympus, Tokyo, Japan). Immunoreactive cells in the pyramidal cell layers of the CA1 and CA3 and in the granule cell layer of the inferior blade of the DG locating within 800 × 600 μm^2 area were counted by an investigator who was not informed of the experimental conditions. A neuron was considered immunoreactive if the nucleus was stained as intensely as those seen within several inner lines of the granule cell layers in the dentate gyrus [14]. For each animal, an averaged value was derived from two independent counts of at least two different sections.

2.4. Statistical analysis

All data were analyzed by parametric analysis of one-way ANOVA for multiple comparisons. Comparisons between groups were adjusted by Bonferroni method. A P value <0.05 was considered to indicate a statistically significant difference.

3. Results

3.1. Freezing behavior to context and to tone cue

Freezing behavior to the context was observed without tone presentation. This behavior is known to depend mostly on the hippocampus [12]. As shown in Fig. 1, there was a significant increase in % freezing time to the context immediately after the footshock both in the young (n = 8, mean ± SEM: 41.251 ± 13.678) and aged footshock rats (n = 7, mean ± SEM: 43.809 ± 25.850) as compared to respective control rats that did not receive footshock (no-footshock rats) (young, n = 5, mean ± SEM: 2.666 ± 5.961; aged, n = 4, mean ± SEM: 2.500 ± 3.317) ($F_{3,20}$ = 10.870, P = 0.0001). However, there was no significant difference between the young footshock rats and the aged footshock rats (P = 0.7687). The no-footshock rats exhibited little or no freezing behavior to the context in either the young or aged group.

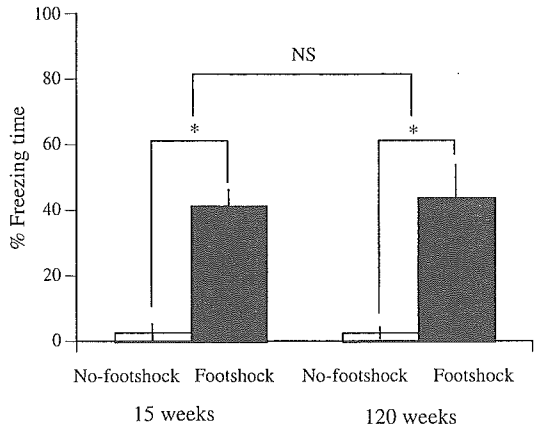

Fig. 1. Percentage freezing time in response to context immediately after footshock. After footshock, rats were allowed to recover for 30 s, and then returned to the home cage. Then, the rats were immediately returned to a conditioning chamber. Freezing behavior was observed for 5 min without CS tone. Both 15-week-old and 120-week-old rats showed freezing behavior in response to the footshock, with no significant difference between young and old rats ($P = 0.7687$). *$P = 0.0001$.

As shown in Fig. 2, at 2 h after the footshock, there was a significant difference in % freezing time during re-exposure to the context (without tone CS) only between the young footshock rats ($n = 8$, mean ± SEM: 31.375 ± 12.856) and the young no-footshock rats ($n = 5$, mean ± SEM: 0.780 ± 1.226) ($P < 0.0001$), and between the young footshock rats and the aged footshock rats (aged footshock, $n = 7$, mean ± SEM: 10.300 ± 8.316; aged no-footshock, $n = 4$, mean ± SEM: 0.975 ± 1.950) ($P < 0.0002$). However, in the aged group, there was no difference between the footshock and the no-footshock rats. The no-footshock control rats exhibited little or no freezing behavior during re-exposure to the context.

Then, the freezing behavior when the rats were re-exposed to the tone cue was observed, which is known to depend on the amygdala [12,26]. Two hours after the footshock, there was a significant increase in % freezing

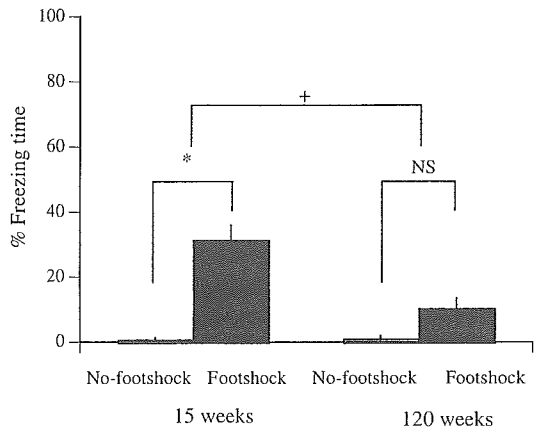

Fig. 2. Percentage freezing time in response to context at 2 h after footshock. Two hours after footshock, rats were once again introduced to a conditioning chamber. The rats' freezing behavior was observed for 5 min only with contextual cue. Under this condition, freezing behavior indicates hippocampus-dependent learning. *$P = 0.0001$. $^{+}P = 0.0002$.

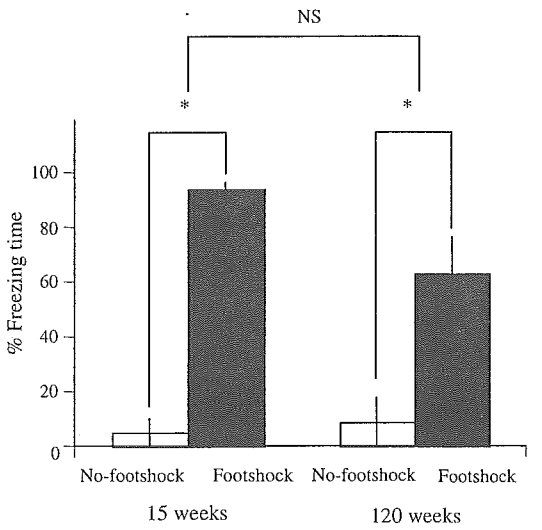

Fig. 3. Percentage freezing time in response to CS tone at 2 h after footshock. Two hours after footshock, rats were once again introduced to the conditioning chamber. They were then observed for the first 5 min with the CS tone. Footshocked rats in both the 15-week-old and 120-week-old groups showed a significant increase in % freezing time compared to the no-footshock control group (*$P < 0.0001$). However, there was no significant difference between the young group and the aged group.

time in both young footshock and aged footshock rats (young, $n = 8$, mean ± SEM: 93.75 ± 2.455; aged, $n = 7$, mean ± SEM: 62.857 ± 13.401) ($F_{3,20} = 23.871$, $P < 0.0001$) as compared to the no-footshock controls (young, $n = 5$, mean ± SEM: 5 ± 5; aged, $n = 4$, mean ± SEM: 8.75 ± 8.85). However, there was no significant difference between the young and aged footshock groups ($P = 0.1119$) (Fig. 3).

3.2. Immunohistochemical study

As shown in Fig. 4, there was no significant difference in the number of non-phosphorylated CREB-immunoreactive

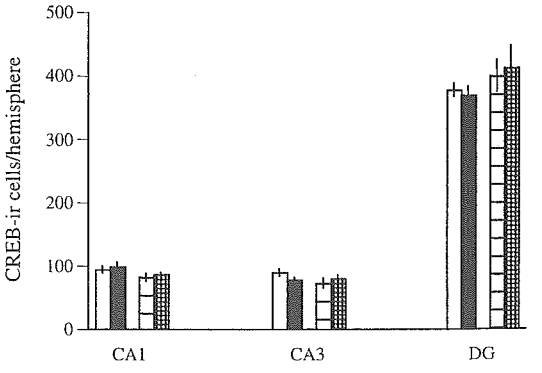

Fig. 4. CREB-immunoreactive cells in hippocampus at 2 h after footshock. White bars represent 15-week-old no-footshock group, solid bars 15-week-old footshock group, striped bars 120-week-old no-footshock group, and hatched bars 120-week-old footshock group. The number of cells expressing the constitutive form of CREB in various areas of the hippocampus is shown. The highest number of CREB-immunoreactive (CREB-ir) cells was found in the dentate gyrus as compared to other parts of the hippocampus, whereas no effect of either footshock or aging was observed.

(CREB-ir) neurons in any area of the hippocampus [(CA1: young no-footshock, n = 5, mean ± SEM: 95.2 ± 5.361; young footshock, n = 8, mean ± SEM: 99.6 ± 6.008; aged no-footshock, n = 4, mean ± SEM: 83 ± 6.151; aged footshock, n = 7, mean ± SEM: 87.5 ± 2.577, $F_{3,20}$ = 1.630, P = 0.241); (CA3: young no-footshock, n = 5, mean ± SEM: 90.6 ± 5.466 young footshock, n = 8, mean ± SEM: 79.125 ± 2.997; aged no-footshock, n = 4, mean ± SEM: 73.25 ± 7.554; aged footshock, n = 7, mean ± SEM: 81 ± 4.88, $F_{3,20}$ = 1.748, P = 1.896); (DG: young no-footshock, n = 5, mean ± SEM: 378.4 ± 10.088; young footshock, n = 8, mean ± SEM: 370 ± 13.649; aged no-footshock, n = 4, mean ± SEM: 401 ± 25.403; aged footshock, n = 7, mean ± SEM: 413.857 ± 34.845, $F_{3,20}$ = 0.781, P = 0.5186)] (Fig. 4).

By immunostaining pCREB, numerous intensely immunostained cells were observed in the hippocampal subregions including the CA3 and the DG in all groups (not shown) (Fig. 5). In contrast, the CA1 area in the no-footshock rats contained only a small number of pCREB-immunoreactive (pCREB-ir) cells. Direct comparison of the distributions of pCREB-ir cells and CREB-ir cells in adjacent hippocampal sections revealed that most of the pCREB-ir cells were also immunoreactive for CREB in the hippocampal subregions except for the CA1. We calculated the ratio of pCREB-ir cell number to CREB-ir cell number in given areas of adjacent sections (expressed as % pCREB-ir cells) as an indicator of CREB phosphorylation.

The % pCREB-ir cells ranged from 74 to 98% in the CA3 and the DG in both the young controls and aged controls, while they were less than 35% in the CA1 (Fig. 6).

At 2 h after the footshock, there was a significant increase of % pCREB-ir cells in the CA1 of the hippocampus in the young rats (CA1: young no-footshock, n = 5, mean ± SEM: 34.600 ± 14.993; young footshock, n = 8, mean ± SEM: 62.875 ± 17.150) ($F_{3,20}$ = 11, P = 0.0002), while no significant difference in % pCREB-ir cells was found in the same area of the aged group (aged no-footshock, n = 4, mean ± SEM: 16.000 ± 12.702; aged footshock, n = 7, mean ± SEM: 27.857 ± 13.741). Thus, an increase of CREB phosphorylation in response to CFC occurred only in the CA1 area of the hippocampus in the young rats. In other hippocampal areas, such as the CA3 and the DG, there was no significant increase in % pCREB-ir cells [(CA3: young no-footshock, n = 5, mean ± SEM: 89.800 ±

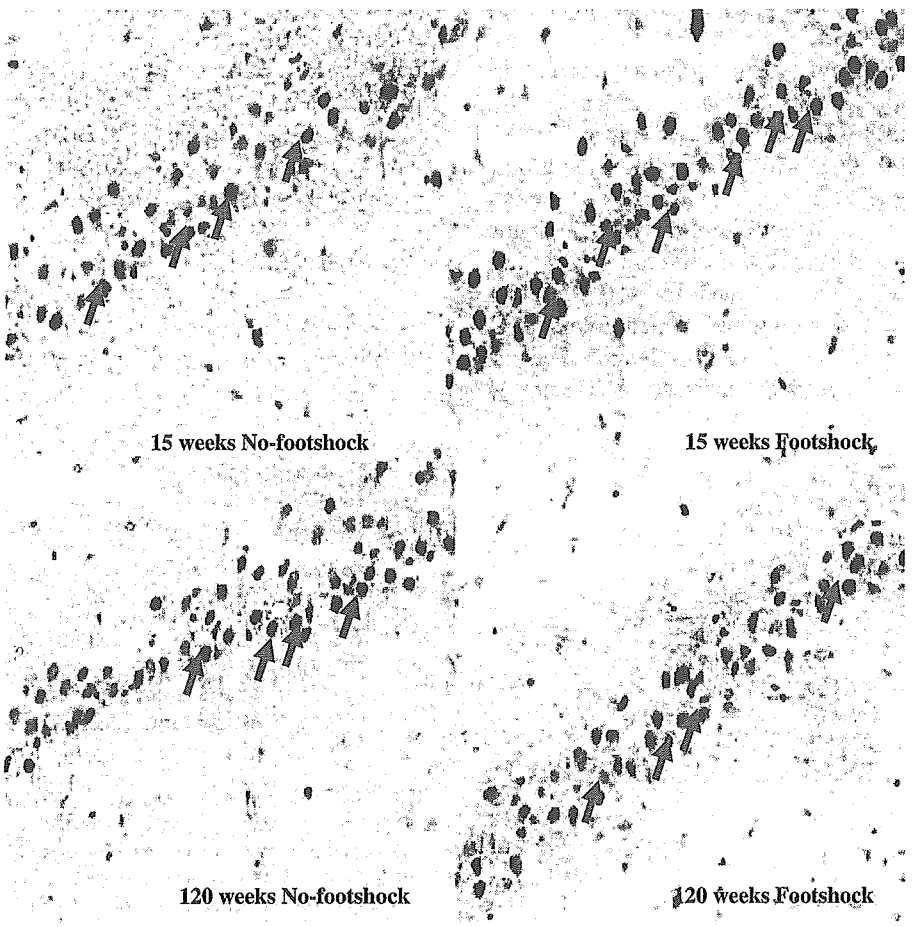

Fig. 5. pCREB-ir cells in CA1 of hippocampus. The cells were specifically immunostained by anti-phosphorylated CREB antibody (pCREB-ir cells, arrows). The number of pCREB-ir cells in the CA1 region of the hippocampus is relatively lower than that in other hippocampal regions. A larger cell population was found in 15-week-old footshocked rats, compared to other groups.

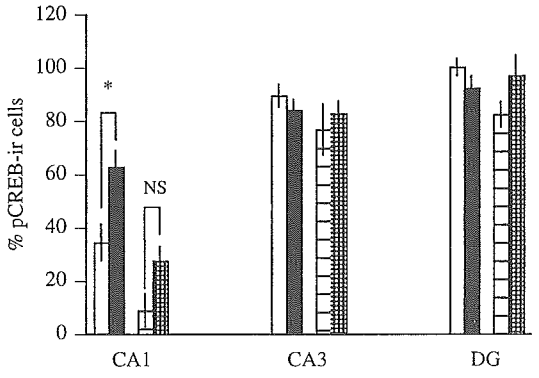

Fig. 6. Percentage of pCREB-immunoreactive cells in hippocampus at 2 h after footshock. White bars represent 15-week-old no-footshock group, solid bars 15-week-old footshock group, striped bars 120-week-old no-footshock group, and hatched bars 120-week-old footshock group. Measurement of pCREB-immunoreactive cells in adjacent brain sections revealed a role of the CA1 in context-dependent learning and the effect of aging. Relative comparison of pCREB-ir cells compared to CREB-ir cells (% pCREB-ir cells) eliminates the bias caused by the difference in cell number. A significant difference was observed between young footshock rats and young non-footshock rats. *P = 0.0002.

9.149; young footshock, n = 8, mean ± SEM: 84.375 ± 11.513; aged no-footshock, n = 4, mean ± SEM: 74.000 ± 26.558; aged footshock, n = 7, mean ± SEM: 83.143 ± 12.158); (DG: young no-footshock, n = 5, mean ± SEM: 100.400 ± 7.369; young footshock, n = 8, mean ± SEM: 92.250 ± 13.134; aged no-footshock, n = 4, mean ± SEM: 87.000 ± 2.309; aged footshock, n = 7, mean ± SEM: 96.857 ± 20.012)] (CA3: P = 0.4657, DG: P = 0.4932). Furthermore, there was no significant difference in % pCREB-ir cells in the basolateral amygdala or the piriform cortex in response to CFC in either the young rats or the aged rats (data not shown).

4. Discussion

Immediately after the footshock, aged rats exhibited freezing behavior in response to contextual stimuli as well as its younger counterparts. Two hours after footshock, no age-related difference was found in response to the tone cue. Since freezing behavior immediately after the footshock was not impaired in aged rats, sensory impairment by aging does not influence footshock-induced freezing behavior. However, the freezing behavior in response not to the tone cue but to the context was impaired in the aged rats. These results imply that there is age-associated disturbance of hippocampal function, while amygdala function is spared. This finding is consistent with reports that aged rats showed impairment of other hippocampus-dependent learning tasks [7,9,20,22,27,30,35]. Previous experiments also showed that lesions in the dorsal hippocampus made 1 day after training impaired contextual learning, while tone cue learning was not affected [2,3,25]. However, the impairment was reduced if the lesions were made long after training [2,3]. This concept goes along with the well-known role of the hippocampus; conversion of short-term memory into long-term memory [13]. Moreover, both cue and contextual learning were lost when the basolateral amygdala was destroyed [3], emphasizing that the amygdala is involved in conditioning of fear responses to simple, modality-specific conditioned stimuli as well as to complex, polymodal stimuli, whereas the hippocampus is mainly involved in fear conditioning situations of complex and polymodal events [3,24].

Two hours after the footshock, there was no significant difference in CREB-positive cells in any area of the hippocampus or in either group. A previous study also showed an increase of pCREB protein with learning, but no change in total CREB protein [34]. Therefore, we regarded % pCREB-ir cells as an indicator for phosphorylation rate of CREB, which is known to be associated with the plasticity of neurons [18,36]. In the no-footshock groups, % pCREB-ir cells was high in the CA3 and the DG, but low in the CA1 in both the young and aged rats. In the young rats, % pCREB-ir cells significantly increased only in the CA1 region of the hippocampus in the footshock group as compared to the no-footshock group. In the aged footshock group, there was no significant difference in % pCREB-ir cells in any area as compared to the no-footshock group.

It was also suggested that CREB phosphorylation induces intracellular protein synthesis in neurons. One of them is BDNF [10], which is involved in the formation of memory through several mechanisms: modification of transmitter release, receptor-mediated responses to neurotransmitters, neuronal circuits, and increased synaptic innervation density [36]. CFC causes a significant increase in BDNF mRNA only in the CA1 region. There is already abundant BDNF in the CA3 and the DG even before conditioning [10]. In addition, the importance of the CA1 in memory has been shown in mutant animals. Mice that lack the NMDA receptor restricted to the CA1 region show a deficit of spatial learning memory [13], and in a human study, damage restricted to just neurons in the CA1 is sufficient to produce memory impairment [18]. These results suggest that the CA1 may have rapid and crucial capacity to process new information and form memory.

In the young footshock group, there was a marked increase of % pCREB-ir cells in the CA1 in response to CFC, as compared to the young no-footshock group, in line with result from another group [12]. pCREB is also selectively recruited in the CA1 in the formation of LTP [29]. Radulovic et al. revealed a high level of FOS protein in the hippocampus after CFC [26]. The same study also demonstrated FOS expression in the amygdala in response to various CFC training, emphasizing the role of this nucleus in CFC-related learning [26]. However, in our study, no increase in pCREB-ir cells was found in the amygdala, suggesting that the role of this nucleus in CFC is not mediated through CREB phosphorylation.

In aged rats, there was significant impairment of CREB phosphorylation in the CA1 as compared to young rats, along with impairment of learning as measured by freezing behavior. It is likely that the age-related impairment of CREB phosphorylation in the CA1 is related to learning impairment. Although the exact mechanism of the age-related impairment of CREB phosphorylation is unknown, there are several possible explanations. This finding may be related to a decrease of NMDA receptors in the CA1 in aged rats [37], since the NMDA receptor has an important role in CREB phosphorylation. The NMDA receptor, when activated, promotes intracellular Ca^{2+} influx and increases cAMP, which triggers CREB phosphorylation. Treatment with MK801, an NMDA antagonist, completely blocks the LTP-related increase of pCREB [29]. Thus, the decrease of NMDA receptors in aged rats may play an important role in attenuating learning and associated impairment of CREB phosphorylation. Alternatively, an increase of intracellular calcium level or long-term exposure to free radicals and/or a high corticosteroid level in aged rats may lead to NMDA receptor dysfunction or altered membrane function, resulting in impairment of CREB phosphorylation [17].

Although our results strongly suggest that in the early process of long-term memory formation, aged male rats exhibit memory impairment as a result of impaired CREB phosphorylation in the CA1, the exact mechanism needs to be solidified in further studies.

Acknowledgments

This study was supported by the Target Oriented Brain Science Promotion Program and a grant from the Japanese Ministry of Culture, Sports and Science (#16390321). The study was also supported by grants from the Japanese Ministry of Health and Labor.

References

[1] C.M. Alberini, M. Ghirardi, Y.Y. Huang, P.V. Nguyen, E.R. Kandel, A molecular switch for the consolidation of long-term memory: cAMP-inducible gene expression, Ann. N. Y. Acad. Sci. 758 (1995) 261–286.

[2] S.G. Anagnostaras, S. Maren, M.S. Fanselow, Temporally graded retrograde amnesia of contextual fear after hippocampal damage in rats: within-subjects examination, J. Neurosci. 19 (1999) 1106–1114.

[3] S.G. Anagnostaras, G.D. Gale, M.S. Fanselow, Hippocampus and contextual fear conditioning: recent controversies and advances, Hippocampus 11 (2001) 8–17.

[4] C.A. Barnes, B.L. McNaughton, An age comparison of the rates of acquisition and forgetting of spatial information in relation to long-term enhancement of hippocampal synapses, Behav. Neurosci. 99 (1985) 1040–1048.

[5] R. Bourtchuladze, B. Frenguelli, J. Blendy, D. Cioffi, G. Schutz, A.J. Silva, Deficient long-term memory in mice with a targeted mutation of the cAMP-responsive element-binding protein, Cell 79 (1994) 59–68.

[6] G. Diana, M.R. Domenici, A. Scotti de Carolis, A. Loizzo, S. Sagratella, Reduced hippocampal CA1 Ca(2+)-induced long-term potentiation is associated with age-dependent impairment of spatial learning, Brain Res. 686 (1995) 107–110.

[7] C.A. Erickson, C.A. Barnes, The neurobiology of memory changes in normal aging, Exp. Gerontol. 38 (2003) 61–69.

[8] M.S. Fanselow, Contextual fear, gestalt memories, and the hippocampus, Behav. Brain Res. 110 (2000) 73–81.

[9] M. Gallagher, J.L. Bizon, E.C. Hoyt, K.A. Helm, P.K. Lund, Effects of aging on the hippocampal formation in a naturally occurring animal model of mild cognitive impairment, Exp. Gerontol. 38 (2003) 71–77.

[10] J. Hall, K.L. Thomas, B.J. Everitt, Rapid and selective induction of BDNF expression in the hippocampus during contextual learning, Nat. Neurosci. 3 (2000) 533–535.

[11] P.C. Holland, M.E. Bouton, Hippocampus and context in classical conditioning, Curr. Opin. Neurobiol. 9 (1999) 195–202.

[12] S. Impey, D.M. Smith, K. Obrietan, R. Donahue, C. Wade, D.R. Storm, Stimulation of cAMP response element (CRE)-mediated transcription during contextual learning, Nat. Neurosci. 1 (1998) 595–601.

[13] E.R. Kandel, Cellular mechanism of learning and the biological basis of individuality, part IX: language, thought, mood, learning and memory, in: J.H.S.E.R. Kandel, T.M. Jessell (Eds.), Principles of Neural Science, McGraw Hill, New York, 2000, pp. 1268–1269.

[14] K. Kudo, C.X. Qiao, S. Kanba, J. Arita, A selective increase in phosphorylation of cyclic AMP response element-binding protein in hippocampal CA1 region of male, but not female, rats following contextual fear and passive avoidance conditioning, Brain Res. 1024 (2004) 233–243.

[15] P.W. Landfield, G. Lynch, Impaired monosynaptic potentiation in in vitro hippocampal slices from aged, memory-deficient rats, J. Gerontol. 32 (1977) 523–533.

[16] P.W. Landfield, J.L. McGaugh, G. Lynch, Impaired synaptic potentiation processes in the hippocampus of aged, memory-deficient rats, Brain Res. 150 (1978) 85–101.

[17] M.A. Lynch, Analysis of the mechanisms underlying the age-related impairment in long-term potentiation in the rat, Rev. Neurosci. 9 (1998) 169–201.

[18] M. Mayford, E.R. Kandel, Genetic approaches to memory storage, Trends Genet. 15 (1999) 463–470.

[19] B.S. McEwen, Stress and the aging hippocampus, Front. Neuroendocrinol. 20 (1999) 49–70.

[20] D.A. Merrill, R. Karim, M. Darraq, A.A. Chiba, M.H. Tuszynski, Hippocampal cell genesis does not correlate with spatial learning ability in aged rats, J. Comp. Neurol. 459 (2003) 201–207.

[21] J.H. Morrison, P.R. Hof, Life and death of neurons in the aging brain, Science 278 (1997) 412–419.

[22] J.A. Oler, E.J. Markus, Age-related deficits on the radial maze and in fear conditioning: hippocampal processing and consolidation, Hippocampus 8 (1998) 402–415.

[23] G. Paxinos, C. Watson, The Rat Brain in Stereotactic Coordinates, 4th ed., Academic Press, Orlando, 1998.

[24] R.G. Phillips, J.E. LeDoux, Differential contribution of amygdala and hippocampus to cued and contextual fear conditioning, Behav. Neurosci. 106 (1992) 274–285.

[25] R.G. Phillips, J.E. LeDoux, Lesions of the dorsal hippocampal formation interfere with background but not foreground contextual fear conditioning, Learn. Mem. 1 (1994) 34–44.

[26] J. Radulovic, J. Kammermeier, J. Spiess, Relationship between fos production and classical fear conditioning: effects of novelty, latent inhibition, and unconditioned stimulus preexposure, J. Neurosci. 18 (1998) 7452–7461.

[27] P. Riekkinen Jr., R. Miettinen, J. Sirvio, M. Aaltonen, P. Riekkinen, The correlation of passive avoidance deficit in aged rat with the loss of nucleus basalis choline acetyltransferase-positive neurons, Brain Res. Bull. 25 (1990) 415–417.

[28] E.D. Roberson, J.D. English, J.P. Adams, J.C. Selcher, C. Kondratick, J.D. Sweatt, The mitogen-activated protein kinase cascade couples PKA and PKC to cAMP response element binding

protein phosphorylation in area CA1 of hippocampus, J. Neurosci. 19 (1999) 4337–4348.
[29] S. Schulz, H. Siemer, M. Krug, V. Hollt, Direct evidence for biphasic cAMP responsive element-binding protein phosphorylation during long-term potentiation in the rat dentate gyrus in vivo, J. Neurosci. 19 (1999) 5683–5692.
[30] J. Shen, C.A. Barnes, B.L. McNaughton, W.E. Skaggs, K.L. Weaver, The effect of aging on experience-dependent plasticity of hippocampal place cells, J. Neurosci. 17 (1997) 6769–6782.
[31] A.J. Silva, J.H. Kogan, P.W. Frankland, S. Kida, CREB and memory, Annu. Rev. Neurosci. 21 (1998) 127–148.
[32] D.E. Smith, P.R. Rapp, H.M. McKay, J.A. Roberts, M.H. Tuszynski, Memory impairment in aged primates is associated with focal death of cortical neurons and atrophy of subcortical neurons, J. Neurosci. 24 (2004) 4373–4381.
[33] T. Tamura, A.S. Chiang, N. Ito, H.P. Liu, J. Horiuchi, T. Tully, M. Saitoe, Aging specifically impairs amnesiac-dependent memory in *Drosophila*, Neuron 40 (2003) 1003–1011.
[34] H. Viola, M. Furman, L.A. Izquierdo, M. Alonso, D.M. Barros, M.M. de Souza, I. Izquierdo, J.H. Medina, Phosphorylated cAMP response element-binding protein as a molecular marker of memory processing in rat hippocampus: effect of novelty, J. Neurosci. 20 (2000) RC112.
[35] J.E. Wallace, E.E. Krauter, B.A. Campbell, Animal models of declining memory in the aged: short-term and spatial memory in the aged rat, J. Gerontol. 35 (1980) 355–363.
[36] M. Walton, C. Henderson, S. Mason-Parker, P. Lawlor, W.C. Abraham, D. Bilkey, M. Dragunow, Immediate early gene transcription and synaptic modulation, J. Neurosci. Res. 58 (1999) 96–106.
[37] G.L. Wenk, C.A. Barnes, Regional changes in the hippocampal density of AMPA and NMDA receptors across the lifespan of the rat, Brain Res. 885 (2000) 1–5.
[38] K. Yamada, Y. Noda, Y. Komori, H. Sugihara, T. Hasegawa, T. Nabeshima, Reduction in the number of NADPH-diaphorase-positive cells in the cerebral cortex and striatum in aged rats, Neurosci. Res. 24 (1996) 393–402.
[39] J.C. Yin, M. Del Vecchio, H. Zhou, T. Tully, CREB as a memory modulator: induced expression of a dCREB2 activator isoform enhances long-term memory in *Drosophila*, Cell 81 (1995) 107–115.

Available online at www.sciencedirect.com
SCIENCE DIRECT®
Neuroscience Research 51 (2005) 31–38
Neuroscience Research
www.elsevier.com/locate/neures

Ginseng enhances contextual fear conditioning and neurogenesis in rats

ChunXiang Qiao[a], Ryousuke Den[b], Koutaro Kudo[a], Kazuo Yamada[a], Keiko Takemoto[c], Henny Wati[a], Shigenobu Kanba[d,*]

[a]*Department of Neuropsychiatry, Interdisciplinary Graduate School of Medicine and Engineering, University of Yamanashi, Japan*
[b]*Department of Neuropsychiatry, Keio University School of Medicine, Tokyo, Japan*
[c]*Graduate School of Nursing, Faculty of Medicine, University of Yamanashi, Japan*
[d]*Department of Neuropsychiatry, Graduate School of Medical Sciences, Kyushu University, 3-1-1 Maidashi, Higashiku, Fukuoka 812-8582, Japan*

Received 18 March 2004; accepted 9 September 2004
Available online 6 November 2004

Abstract

Panax Ginseng is a commonly used galenical known to have an enhancing effect on learning. Neurogenesis in the hippocampus has been shown to be necessary for hippocampus/amygdala-dependent learning tasks. To investigate the role of Ginseng in neurogenesis and learning of rats, we administered both Ginseng and BrdU for five consecutive days. As a result, Ginseng increased the number of BrdU-positive cells in the dentate gyrus in a dose-dependent manner. Further, we administered one dose of BrdU after Ginseng treatment for five consecutive days, and the number of BrdU-positive cells did not increase significantly. However, when one dose of BrdU was given 1 day before the following five consecutive days of Ginseng treatment, the number of BrdU-positive cells markedly increased in the hippocampus. Therefore, it is likely that Ginseng enhances not proliferation but survival of newly generated neurons in the hippocampus. Second, we administered both Ginseng and BrdU to rats for five consecutive days. One day after the last Ginseng and BrdU co-administration, contextual fear conditioning (CFC) was conducted. Ginseng in a dose-dependent manner increased the % freezing time and the number of BrdU-positive cells in the dentate gyrus of rats that received CFC. Thus, an increase in CFC-related neurogenesis may be one mechanism of Ginseng's properties to enhance learning ability.
© 2004 Published by Elsevier Ireland Ltd and the Japan Neuroscience Society.

Keywords: Ginseng; Neurogenesis; Learning; Hippocampus; Dentate gyrus; Contextual fear conditioning

1. Introduction

The Ginseng root (Panax Ginseng) is a common constituent of a large number of traditional oriental medicines. Among its diverse effects on the central nervous system, Ginseng is known to improve learning and memory. Although some of the early studies reported that Ginseng extracts caused learning impairment rather than improvement (Saito et al., 1977, 1979), subsequent studies showed that Ginseng extracts improve performance in active and passive avoidance learning tasks (Lasarova et al., 1987; Petkov et al., 1990, 1992, 1993). This discrepancy may be due to the sedative effect of Ginseng (Koo, 1999), which is observed with acute administration of Ginseng. Those that reported memory impairment by Ginseng examined the acute, but not chronic effects of Ginseng.

Chronic administration of Ginseng extracts or some of its fractions is known to improve learning and memory in several different hippocampus/amygdala-dependent behavioral tasks (Chang et al., 1998; Jaenicke et al., 1991; Jin et al., 1999; Lyubimov et al., 1997; Ni et al., 1993; Nitta et al., 1995a, 1995b; Watanabe et al., 1990; Wen et al., 1996; Yoshimura et al., 1998; Zhao and McDaniel, 1998; Zhong et al., 1998). However, the molecular and cellular mechanisms by which these agents exert behavioral effects remain to be explored.

In recent years, neurogenesis in the subgranular layer of the hippocampus (Gould et al., 1999b) and subsequent

* Corresponding author. Tel.: +81 92 642 5620; fax: +81 92 642 5644.
E-mail address: skanba@npsych.med.kyushu-u.ac.jp (S. Kanba).

0168-0102/$ – see front matter © 2004 Published by Elsevier Ireland Ltd and the Japan Neuroscience Society.
doi:10.1016/j.neures.2004.09.004

enhancement of neurotract connections (Nakagawa et al., 2002b) have drawn attention as one of the molecular biological mechanisms of hippocampus/amygdala-dependent learning. The hippocampus is one of few brain regions where production of neurons occurs throughout the lifetime of animals, including humans. Gould et al. (1999a) reported that improvement of a hippocampus-dependent task, such as a spatial learning test, was associated with increase in survival of bromodeoxyuridine (BrdU)-positive cells in rats.

To clarify the mechanism of learning enhancement by Ginseng, we investigated the effects of Ginseng on contextual fear conditioning (CFC), a hippocampus/amygdala-dependent learning task, and on neurogenesis in the hippocampus of rats. Prior to this investigation, we examined the effect of Ginseng on the baseline number of BrdU-positive cells in the hippocampus. For analysis of the phenotype of BrdU-positive cells, double staining with BrdU, a thymidine analog that labels dividing cells in S-phase, and NeuN, a neuronal marker, was used.

2. Materials and methods

2.1. Animals and Ginseng treatment

All experiments were conducted using 60 adult male Wister/ST rats (SLC Japan, 9 weeks old, weighing 270–290 g). They were group-housed (5 rats/group, 12 h light/dark cycle) with ad libitum access to food and water. The animals were treated in accordance with the Guidelines for Animal Experimentation (of the Ethics Review Committee) of the Faculty of Medicine, University of Yamanashi.

For the first experiment, Ginseng powder (supplied by Tsumura Pharmaceutical Co., Tokyo, Japan) was administered orally at doses of 0, 100, and 200 mg/kg/day for five successive days via a gastric tube. Dried Ginseng powder was suspended in tap water just before the use. The group denoted as 0 mg/kg/day received water only. Although in some previous reports Ginseng was administered by intraperitoneal (Mook-Jung et al., 2001) or intracerebroventricular injection (Kim et al., 1998), we considered that oral administration of Ginseng was crucial, because in traditional medicine Ginseng has always been taken orally. In addition, no data are available regarding the disposition of Ginseng in the body, such as absorption and metabolism, and more importantly, biologically active forms are not well identified. Some herbs are known to be metabolized into active forms by intestinal bacteria and then absorbed to exert pharmacological actions (Hasegawa et al., 1996). Thus, non-oral administration of Ginseng may result in non-pharmacological artifacts.

2.2. Contextual fear conditioning

CFC was conducted according to the method of Silva et al. (1998). The CFC task was performed in a conditioning chamber housed in a sound-attenuating box during the light phase of the cycle. The conditioning chamber (28 cm (width) × 21 cm (height) × 22 cm (diameter)) was constructed of clear Plexiglas. The floor of the chamber was lined with 18 stainless steel bars (4 mm in diameter; 1.5 cm spacing), which formed a foot shock grid to deliver scrambled shocks produced by a stimulator. The foot shock was 2 s direct current of 0.75 mA and served as the aversive unconditioned stimulus. The sound-attenuating box (48 cm (width) × 48 cm (height) × 48 cm (diameter)) was provided with a 20 W houselight, and a ventilation fan supplying background white noise (74 dB) was located on the top of the box. A discrete tone conditioned stimulus (CS) was given as a general contextual stimulus. The tone cue (800 Hz, 20 s duration, 80 dB) was delivered by two speakers located in the lower corner of the sound-attenuating box.

Prior to the conditioning, all rats received 3 days of habituation, in which they were placed in the conditioning chamber for 1 min and returned to their home cages once a day. On the day of conditioning, the rats were placed in the conditioning chamber and allowed to explore for 3 min. A foot shock was delivered 18 s after the tone CS. The rats were then allowed to recover for 30 s in the conditioning chamber and returned to their home cages. Two hours later, the rats were again introduced into the conditioning chamber and were tested for a 5 min period, during which no tone CS was delivered. Behavior was evaluated in terms of total freezing time during a 5 min (% freezing time) stay in the conditioning chamber. Freezing behavior was defined as cessation of all but respiratory movement. The rats were sacrificed immediately after % freezing time was measured.

Rats that experienced footshock were allocated to the CFC group and rats that did not experience footshock to the no-CFC group. There were three subgroups in the CFC and no-CFC groups, each of which was treated with 0, 100, or 200 mg/kg/day Ginseng powder. There were five rats in each subgroup.

2.3. Open field locomotion test

To test whether % freezing time was influenced by the sedative effect of Ginseng or not, the open field locomotion test was performed at the end of the treatment period on the sixth day. This test was performed on the rats that were administered 0 or 200 mg/kg/day of Ginseng.

The open field is a 750 mm× 750 mm wooden arena, with 300 mm high walls surrounding the field, painted black on all inner surfaces. Thin white stripes are painted across the floor, dividing it into 25 quadratic blocks. The open field instrument was cleaned after each individual test session to prevent the next rat from being influenced by the odors deposited in the urine and feces of the previous rat.

The rat was placed in the area with its head pointing to a corner. An observer manually quantified the rat's spontaneous ambulatory locomotion in the horizontal plane by

scoring the number of squares entered (crossing into a different adjacent section with all four extremities), during 5 min.

2.4. Immunostaining

On the sixth day, immediately after CFC performance, the rats were deeply anesthetized with sodium pentobarbital (50 mg/kg ip) and perfused transcardially with 350 ml of 4% paraformaldehyde in 0.1 M phosphate buffer. The rat brain was quickly removed, and then post-fixed for 24 h in paraformaldehyde. Then, 40 μm-thick frontal sections were cut on a cryostat and collected in PBS (0.1 M; pH 7.4). In accordance with the rat brain map of Paxinos and Watson (1986), 40 μm-thick free-floating sections were prepared, and 12 sections were collected at 160 μm intervals for staining. DNA denaturation was conducted by incubation for 30 min in 50% formamide/2 × SSC at 65 °C followed by several rinses in 2 × SSC. Sections were then incubated for 30 min in 2N HCl and 10 min in boric acid. After washing in PBS, sections were incubated in 3% H_2O_2 to block endogenous peroxidase for 10 min. After blocking with 10% normal goat serum (NGS), sections were incubated with anti-BrdU (1:1000 Haralan Sera Lab. OBT0030) for 24 h at 4 °C. Sections were then incubated for 1 h with secondary antibody (biotinylated goat, anti-rat IgG; Vector BA9400) followed by amplification with an avidin–biotin complex, before developing the color using DAB.

The same number of free-floating sections from the control and the Ginseng (200 mg/kg/day for 5 days)-treated animals ($n = 6$) surviving 4 weeks after administration of one dose of BrdU before Ginseng treatment was used for analysis of phenotypes. Double immunostaining procedures with fluorescent chromogens were used to evaluate the co-expression of BrdU with neuronal nuclear protein NeuN. In the double-labeling experiment, BrdU was visualized with Streptavidin-Texas Red (Amersham Pharmacia Biotech, 1:100), while the neuronal marker NeuN (Chemicon International Inc., MAB377; 1:500) was visualized with FITC (anti-mouse Ig, fluorescein-linked whole antibody 1:20). Fluorescent signals were viewed using a TCS4D confocal laser-scanning microscope. The emission signals of Texas Red and FITC were assigned to red and green, respectively.

2.5. Quantification of BrdU labeling

Every fourth section throughout the hippocampus was processed for BrdU immunohistochemical study. All BrdU-labeled cells in the dentate gyrus (granular cell layer) and the hilus were counted in each section. To distinguish single cells within clusters, all counts were performed at 400× and 1000× magnification under a light microscope (Olympus BX-60), omitting cells in the outermost focal plane.

A cell was counted as being in the subgranular zone (SGZ) of the dentate gyrus if it was touching or in the SGZ. Cells that were located more than two cells away from the SGZ were classified as hilar cells. The cell number was divided by the area of the dentate gyrus, and then the mean positive cell number per square millimeter was counted.

2.6. Protocol of BrdU administration

To investigate the overall effects of Ginseng on neurogenesis in the dentate gyrus of rats and its association with CFC performance, rats were orally administered both Ginseng (0, 100, 200 mg/kg/day) and BrdU (200 mg/kg/day) simultaneously for five consecutive days. On the sixth day, the animals were subjected to CFC test and then sacrificed for immunohistochemical study as described above (Fig. 1A).

BrdU is taken up into cells that are in the S-phase of DNA synthesis. The S-phase lasts for approximately 2 h (Packard et al., 1973). When one dose of BrdU is given, it is incorporated only into cells in the S-phase. At least one cell cycle is completed in 24 h by cells in the S-phase after the time of BrdU injection (Nowakowski et al., 1989). Therefore, if an animal is given one dose of BrdU and decapitated 2 h later for immunostaining, cells that have newly proliferated are observed. On the contrary, if an animal is given one dose of BrdU and is decapitated a few days later, cells that were produced a few days ago and are still surviving at the time of decapitation are observed. Accordingly, it is possible to differentiate newly proliferated cells from surviving cells by varying the time interval between BrdU administration and decapitation.

In our study, to determine the effects of Ginseng on cell survival, BrdU was given once to drug-naive rats, and Ginseng was given for the following 5 days. Then, the rats were sacrificed for immunohistochemical study (Fig. 1B). On the other hand, to determine the effects of Ginseng on cell proliferation, BrdU was given once on the sixth day, after Ginseng treatment for five consecutive days, and sacrificed 2 h after BrdU labeling (Fig. 1C).

2.7. Statistical analysis

All the results are presented as mean ± S.E.M. One-way analysis of variance (ANOVA) was used to examine the effects of CFC and Ginseng administration on % freezing time because of their interaction, since there was interaction between the two groups (Fig. 6). Two-way analysis of variance (ANOVA) was used to examine the effect of CFC and Ginseng on number of BrdU-positive cells in rats subjected to CFC (Fig. 2). As shown in Fig. 5, Student's *t*-test was used to determine whether the effect of Ginseng treatment on the number of BrdU-positive cells is related to cell proliferation or cell survival. Differences in the values of locomotion measured in the open field test were examined by Student's *t*-test.

A P-value < 0.05 was considered to indicate a statistically significant difference.

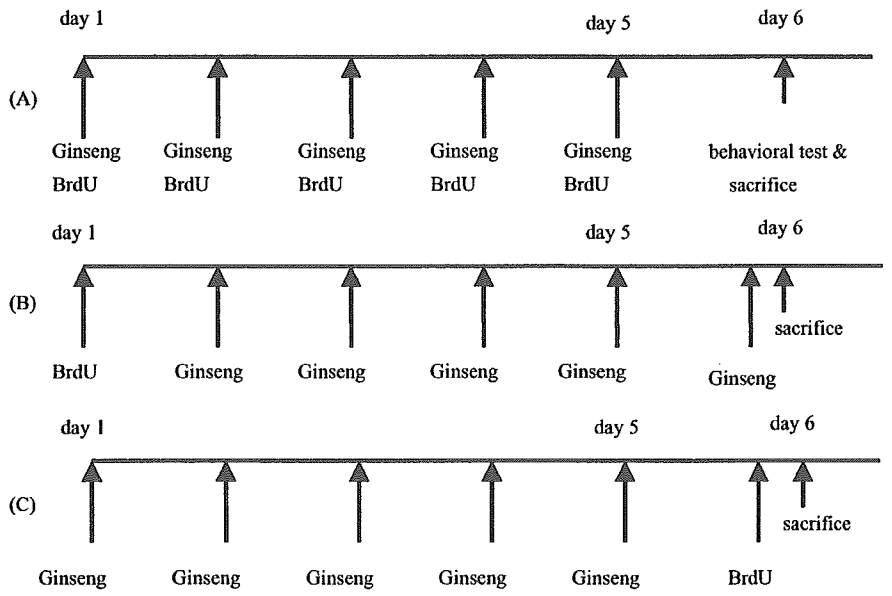

Fig. 1. Experimental procedures to examine effects of Ginseng on CFC-associated neurogenesis, cell survival and cell proliferation in rat hippocampus. Rats were orally administered both Ginseng (0, 100, 200 mg/kg/day) and BrdU (200 mg/kg/day) for five consecutive days. On the sixth day, the animals were subjected to CFC test (A). To determine the effects of Ginseng on cell survival, BrdU was given once to drug-naive rats, and Ginseng was given for the following 5 days. (B) To determine the effects of Ginseng on cell proliferation, BrdU was given once on the sixth day, after Ginseng treatment for five consecutive days, and sacrificed 2 h after BrdU labeling (C).

3. Results

3.1. Effect of Ginseng on baseline number of BrdU-positive cells

To test the effect of Ginseng on neurogenesis in rats, we counted the number of BrdU-positive cells in the dentate gyrus. The number of BrdU-positive cells increased in a dose-dependent manner in the Ginseng treatment group (Figs. 2A and 3).

3.2. Phenotype of BrdU-positive cells

The phenotype of the BrdU-positive cells in the granule cell layer was examined in the Ginseng group 4 weeks after BrdU labeling. We performed immunostaining for BrdU as

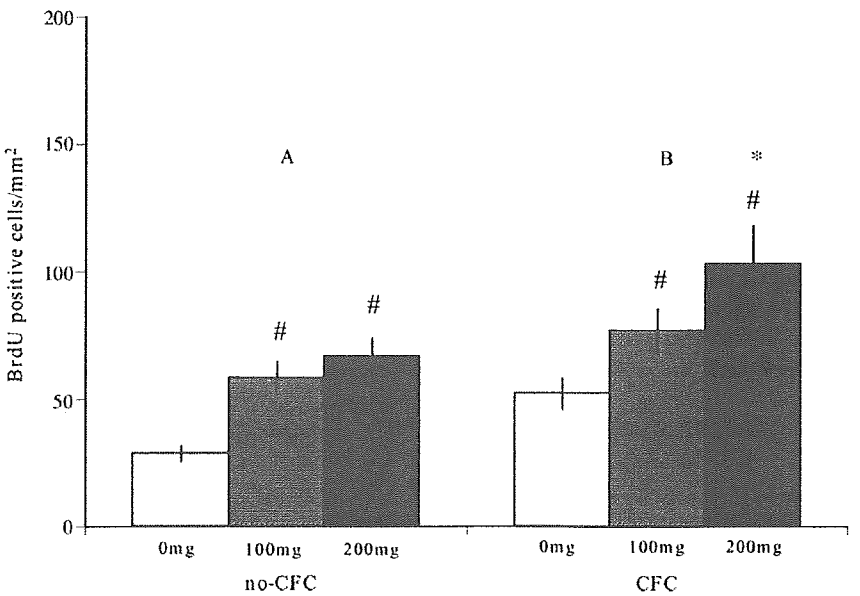

Fig. 2. Change in BrdU-positive cells in rat hippocampus after CFC performance. The number of BrdU-positive cells was higher in the CFC groups than in the no-CFC groups ($P = 0.0113$, $F_{1,24} = 13.718$). The number of BrdU-positive cells was significantly increased in a dose-dependent manner by Ginseng treatment, both in the no-CFC groups (A) and the CFC groups (B) ($P = 0.0001$, $F_{2,24} = 13.538$) (mean ± S.E.M.). (#) $P < 0.05$ vs. 0 mg; (*) $P < 0.05$ for no-CFC vs. CFC.

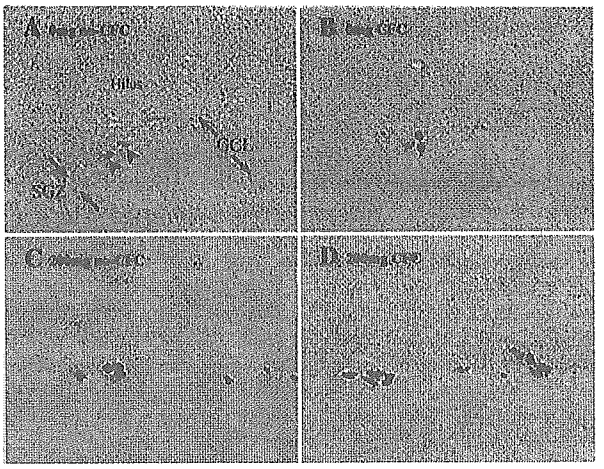

Fig. 3. Optical photomicrographs of changes in number of BrdU-positive cells in the hippocampus after CFC (40× magnification) BrdU-positive cells (arrowhead) were increased in the CFC groups (B and D) compared to the no-CFC groups (A and C). BrdU-positive cells were increased in a dose-dependent manner by Ginseng, in both the CFC groups and no-CFC groups. (A) Ginseng 0 mg and no-CFC; (B) Ginseng 0 mg and CFC; (C) Ginseng 200 mg and no-CFC; (D) Ginseng 200 mg and CFC. The majority of BrdU-positive cells were located in the subgranular zone (SGZ) of the hippocampus—the region between the granular cells layer (GCL) and hilus.

well as for NeuN, a marker for neurons (Fig. 4). It was found that ~80% of BrdU-positive cells expressed NeuN, and no significant difference existed in % NeuN-positive cells regardless of whether Ginseng was administered or not (data not shown).

3.3. Effect of Ginseng on cell survival

The increased neurogenesis may have been due to an increase in cell survival and/or cell proliferation. To investigate the effect of Ginseng specifically on cell survival, one dose of BrdU was given orally to the rats, followed by 5 days' administration of Ginseng (200 mg/kg/day). As a result, Ginseng did significantly increase the number of BrdU-positive cells. This finding showed that Ginseng enhanced the survival rate of newly generated cells in the hippocampus (see Fig. 5A).

3.4. Effect of Ginseng on cell proliferation

On the other hand, in order to investigate the effect of Ginseng on cell proliferation, Ginseng (200 mg/kg/day) was given for 5 days, and then one dose of BrdU was given to the rats 2 h before they were sacrificed for immunostaining. With this administration protocol, the number of BrdU-positive cells did not increase significantly in the dentate gyrus. This result suggested that the Ginseng employed in our experiment did not induce a significant change in cell proliferation in the hippocampus (see Fig. 5B).

3.5. Effect of Ginseng on % freezing time in CFC test and CFC-associated increase in BrdU-positive cells

As shown in Fig. 6A, in the rats that were not given foot shocks in the conditioning chamber (no-CFC group), Ginseng administration did not change % freezing time at any dose. CFC itself increased % freezing time. In the rat groups that received CFC (CFC groups), Ginseng treatment increased % freezing time in a dose-dependent manner (see Fig. 6B). Ginseng at 200 mg/kg significantly increased % freezing time as compared to Ginseng at 0 or 100 mg/kg. This result shows that Ginseng significantly enhances the performance of rats in the CFC, a hippocampus/amygdala-dependent learning task.

When Ginseng and BrdU were co-administered for five consecutive days, the number of BrdU-positive cells increased in a dose-dependent manner in the CFC groups, and the increase was significant at a dose of Ginseng of 200 mg/kg as compared to doses of 0 and 100 mg/kg (Figs. 2B and 3). CFC also increased the number of BrdU-positive cells as compared to the no-CFC groups, even when saline was co-administered with BrdU for 5 days (Figs. 2 and 3).

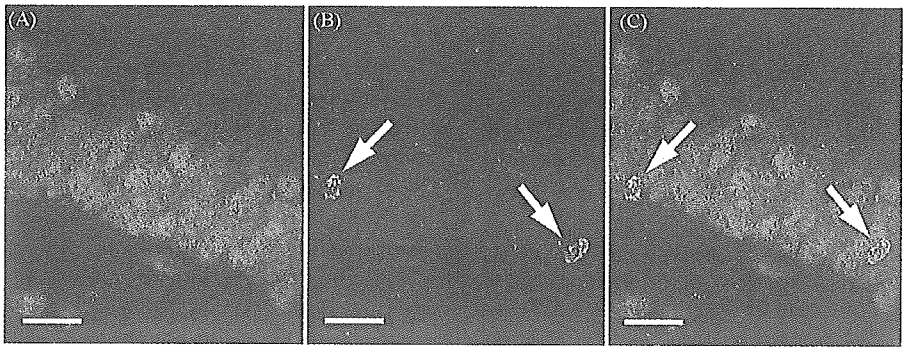

Fig. 4. Double immunolabeling of NeuN and BrdU in adult dentate gyrus of Ginseng-treated rats. Double immunolabeling of NeuN (green, A), a marker of mature neurons, and BrdU (red, B) in the adult dentate gyrus of Ginseng-treated rats surviving 4 weeks after BrdU administration. Confocal images (630× magnification) show NeuN immunoreactivity in BrdU-labeled cells (arrows, C) in both Ginseng-treated and non-treated animals. Scale bar: 20 μm.

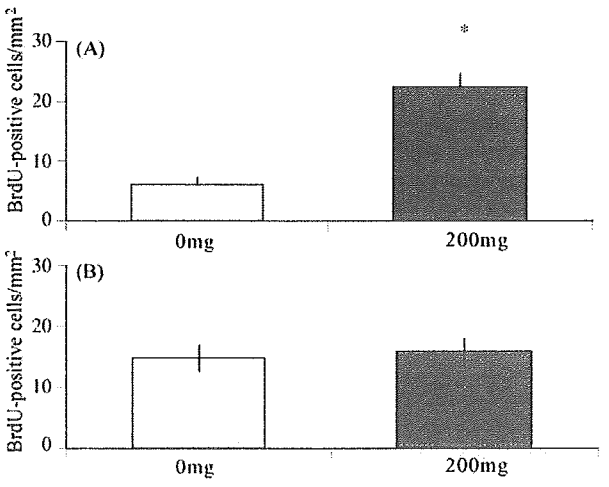

Fig. 5. Effects of Ginseng on BrdU-positive cells in rat hippocampus administration of Ginseng for five consecutive days after one treatment with BrdU significantly increased BrdU-positive cells compared to control rats ($n = 5$, $^{*}P = 0.0003$) (A). Administration of Ginseng for five consecutive days followed by one treatment with BrdU 24 h later caused no significant change in BrdU-positive cells compared to control rats ($n = 5$, $P = 0.7341$) (B).

3.6. Effect of Ginseng on open field locomotion

To examine whether % freezing time was influenced by the sedative effect of Ginseng, the open field test was performed. Total locomotion distance of the group treated with Ginseng 200 mg/kg/day for five consecutive days was not significantly different compared to the no Ginseng group (data not shown). There was no significant difference in grooming and rearing either (data not shown). This result indicates that Ginseng at 200 mg/kg did not cause any difference in spontaneous activity or locomotion compared with the non-treated rats.

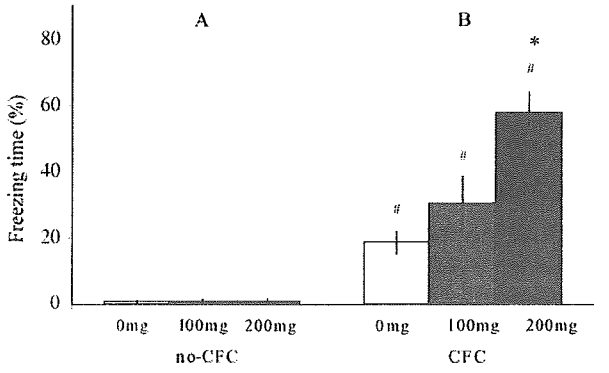

Fig. 6. Effects of Ginseng on % freezing time of rats tested in a conditioning chamber 1 day after finishing administration of Ginseng with BrdU for five consecutive days. Data are shown as mean ± S.E.M. There was a significant difference in % freezing time among the tested groups ($F_{5,24} = 25.312$, $P < 0.007$). (#) The 0, 100, and 200 mg Ginseng groups showed a significantly higher % freezing time in the CFC group than the no-CFC group, respectively. (*) The 200 mg/kg Ginseng group showed the highest % freezing time out of all the CFC groups (B). In contrast, the no-CFC groups did not show any change in % freezing time (A).

4. Discussion

Ginseng administration increased the number of BrdU-positive cells of the dentate gyrus in the no-CFC groups in a dose-dependent manner. Double staining with BrdU and NeuN suggested that the increase in BrdU-labeled cells may be mainly based on an increase in neurogenesis, and not gliogenesis.

Neurogenesis, defined as the creation of new nerve cells, consists of a series of distinct developmental steps, two of which can be examined separately; proliferation and survival/differentiation (Malberg et al., 2000). Our study suggested that the increased number of BrdU-positive cells induced by Ginseng was due to an increase in cell survival, and not cell proliferation.

We also found enhancing effects of Ginseng on performance in CFC, which is hippocampus/amygdala-dependent learning, as well as on neurogenesis in the dentate gyrus in the CFC groups. The unaltered result of the open field test in the Ginseng group shows that Ginseng causes neither a stimulating nor sedating effect at the doses employed in this study, which could potentially interfere with evaluation of CFC. Another interfering factor in evaluation of CFC is that Ginseng's effect on pain sensitivity. Since there is no previous data to suggest this effect, the possibility is low, but still remains to be examined.

Ginseng increased the CFC-related increase in the number of BrdU-positive cells in a dose-dependent manner. Although in this study we did not examine whether this CFC-related increase in the number of BrdU-positive cells was due to increased cell proliferation or cell survival, a previous study suggested that learning was associated with enhancement of cell survival but not cell proliferation (Fulder, 1981; Gould et al., 1999a), although it remains to be answered whether Ginseng and CFC have an additive or interactive effect on neurogenesis. It is reasonable to conclude that the increase in CFC-related neurogenesis may be one mechanism of Ginseng's property to enhance learning ability.

What are the molecular mechanisms underlying the regulation of hippocampal neurogenesis by Ginseng? Ginseng root consists of two major constituents: crude Ginseng saponin and crude Ginseng non-saponin fractions. To date, more than 20 saponins have been isolated from Ginseng root and identified chemically (Lim et al., 1997). Ginsenosides (the saponin constituents of Ginseng root) have been reported to have a number of actions on the CNS. These include CNS stimulation or depression (Watanabe et al., 1990), anticonvulsant activity (Gupta et al., 2001), anti-psychotic activity (Yoshimura et al., 1998), anti-fatigue (Wang et al., 1983) and anti-stress activity (Fulder, 1981; Kim et al., 1998), and improvement of performance in various memory paradigms (Jin et al., 1999; Ni et al., 1993; Nitta et al., 1995a).

The beneficial effects of Ginseng on learning and memory have often been attributed to ginsenoside Rb1

and Rg1 (Mook-Jung et al., 2001). Ginsenoside Rg1 increases cAMP level and c-fos gene expression in the rat hippocampus (Liu and Zhang, 1996). The elevation of intracellular cAMP level induces c-fos expression (Vaccarino et al., 1993). The cAMP–CREB cascade could contribute to the actions of neurotransmitters and neurotrophic factors on adult neurogenesis (Nakagawa et al., 2002a). In recent reports, CREB was shown to be necessary for both steps of neurogenesis: proliferation and cell survival (Nakagawa et al., 2002b). Since in our study, Ginseng did not enhance cell proliferation, activation of the cAMP-CREB cascade by Ginseng could not solely explain our findings.

Alternatively, the ginsenosides Rb1 and Rg1 (Mook-Jung et al., 2001) are also thought to enhance learning and memory by facilitation of cholinergic function, which is apparently essential for the functional integration of learning processes. For example, Rb1 facilitated acetylcholine (ACh) release and improved passive avoidance learning (Benishin et al., 1991). Rb1 and Rg1 increased the number of ACh receptors and improved passive avoidance learning in anisodine-treated mice (Shan et al., 2002). Rg1 improved the performance of scopolamine-injected rats in an eight-arm radial maze task. Consistent with these results, Rb1 facilitated choline uptake and increased choline acetyltransferase (Salim et al., 1997). ACh is also shown to increase neurogenesis (Ma et al., 2000). Thus, the increase of neurogenesis by Ginseng may be mediated via an increase in ACh release and ACh receptors.

In conclusion, Ginseng had an enhancing effect on CFC and increased the number of BrdU-positive cells in the dentate gyrus. The increase of neurogenesis by Ginseng was due to enhancement of cell survival, and not proliferation. Future study will be required to determine the components of Ginseng that are responsible for the enhancement of CFC and neurogenesis. Elucidation of the exact components and their mechanisms will lead to novel drugs for the treatment of memory impairment.

Acknowledgements

We thank Tsumura Pharmaceutical Company, Tokyo, Japan for donating Ginseng. We are grateful to Professor J. Arita (Department of Physiology, Yamanashi University) for his technical advice and critical reading of the manuscript. This study was supported by Target Oriented Brain Science Promotion Program supported by Japanese Ministry of Culture, Sports and Science.

References

Benishin, C.G., Lee, R., Wang, L.C., Liu, H.J., 1991. Effects of ginsenoside Rb1 on central cholinergic metabolism. Pharmacology 42, 223–229.

Chang, Y.S., Wu, C.R., Ho, Y.L., Hsieh, M.T., 1998. Effects of Panax Ginseng and its constituents on drug-induced memory impairment in rats. In: Proceedings of the Seventh International Symposium on Ginseng. pp. 289–299.

Fulder, S.J., 1981. Ginseng and the hypothalamic–pituitary control of stress. Am. J. Chin. Med. 6, 112–118.

Gould, E., Beylin, A., Tanapat, P., Reeves, A., Shors, T.J., 1999a. Learning enhances adult neurogenesis in the hippocampal formation. Nat. Neurosci. 2, 260–265.

Gould, E., Tanapat, P., Hastings, N., Shors, T.J., 1999b. Neurogenesis in adulthood: a possible role in learning. Trends Cog. Neurosci. 3, 186–192.

Gupta, Y.K., Sharma, M., Chaudhary, G., 2001. Antiepileptic activity of Panax Ginseng against pentylenetetrazole induced kindling in rats. Indian J. Physiol. Pharmacol. 45, 502–506.

Hasegawa, H., Sung, J.H., Matsumiya, S., Uchiyma, M., 1996. Main Ginseng saponin metabolites formed by intestinal bacteria. Planta Med. 62, 453–457.

Jaenicke, B., Kim, E.J., Ahn, J.W., Lee, H.S., 1991. Effect of Panax Ginseng extract on passive avoidance retention in old rats. Arch. Pharm. Res. 14, 25–29.

Jin, S.H., Park, J.K., Nam, K.Y., Park, S.N., Jung, N.P., 1999. Korean red Ginseng saponins with low ratios of protopanaxdiol and protopanaxatriol saponin improve scopolamine-induced learning disability and spatial working memory in mice. J. Ethnopharmacol. 166, 123–129.

Kim, D.H., Jung, J.S., Suh, H.W., Huh, S.O., Min, S.K., Son, B.K., Park, J.H., Kim, N.D., Kim, Y.H., Song, D.K., 1998. Inhibition of stress-induced plasma corticosterone levels by ginsenosides in mice: involvement of nitric oxide. Neuroreport 9, 2261–2264.

Koo, M.W., 1999. Effects of Ginseng on ethanol induced sedation in mice. Life Sci. 64, 153–160.

Lasarova, M.B., Mosharrof, A.H., Petkov, V.D., Markovska, V.L., Petkov, V.V., 1987. Effect of piracetam and of standardized Ginseng extracts on the electroconvulsive shock-induced memory disturbances in "step-down" passive avoidance. Acta Physiol. Pharmacol. Bulg. 13, 11–17.

Lim, J.H., Wen, T.C., Matsuda, S., Tanaka, J., Maeda, N., Peng, H., Aburaya, J., Ishihara, K., Sakanaka, M., 1997. Protection of ischemic hippocampal neurons by ginsenoside Rb1, a main ingredient of Ginseng root. Neurosci. Res. 28, 191–200.

Liu, M., Zhang, J.T., 1996. Effects of ginsenoside Rg1 on c-fos gene expression and cAMP levels in rat hippocampus. Zhongguo Yao Li Xue Bao 17, 171–174.

Lyubimov, I.I., Borzenkov, V.M., Chepurnova, N.E., Epurnova, S., 1997. Effect of a polysaccharide fraction of Ginseng root on learning and memory in rats. Neurosci. Behav. Physiol. 27, 555–558.

Ma, W., Maric, D., Li, B.S., Hu, Q., Andreadis, J.D., Grant, G.M., Liu, Q.Y., Shaffer, K.M., Chang, Y.H., Zhang, L., Pancrazio, J.J., Pant, H.C., Stenger, D.A., Barker, J.L., 2000. Acetylcholine stimulates cortical precursor cell proliferation in vitro via muscarinic receptor activation and MAP kinase phosphorylation. Eur. J. Neurosci. 4, 1227–1240.

Malberg, J.E., Eisch, A.J., Nestler, E.J., Duman, R.S., 2000. Chronic antidepressant treatment increases neurogenesis in adult rat hippocampus. J. Neurosci. 24, 9104–9110.

Mook-Jung, I., Hong, H.S., Boo, J.H., Lee, K.H., Yun, S.H., Cheong, M.Y., Joo, I., Huh, K., Jung, M.W., 2001. Ginsenoside Rb1 and Rg1 improve spatial learning and increase hippocampal synaptophysin level in mice. J. Neurosci. Res. 1563, 509–515.

Nakagawa, S., Kim, J.E., Lee, R., Malberg, J.E., Chen, J., Steffen, C., Zhang, Y.J., Nestler, E.J., Duman, R.S., 2002a. Regulation of neurogenesis in adult mouse hippocampus by cAMP and cAMP response element-binding protein. J. Neurosci. 22, 3673–3682.

Nakagawa, S., Kim, J.E., Lee, R., Chen, J., Fujioka, T., Malberg, J., Tsuji, S., Duman, R.S., 2002b. Localization of phosphorylated cAMP response element-binding protein in immature neurons of adult hippocampus. J. Neurosci. 22, 9868–9876.

Ni, X.H., Ohta, H., Watanabe, H., Matsumoto, K., 1993. Panax Ginseng extract improves scopolamine-induced deficits in working memory

performance in the T-maze delayed alternation task in rats. Phytother. Res. 7, 49–52.

Nitta, H., Matsumoto, K., Shimizu, M., Ni, X.H., Watanabe, H., 1995a. Panax Ginseng extract improves the performance of aged Fischer 344 rats in radial maze task but not in operant brightness discrimination task. Biol. Pharm. Bull. 18, 1286–1288.

Nitta, H., Matsumoto, K., Shimizu, M., Ni, X.-H., Watanabe, H., 1995b. Panax Ginseng extract improves the scopolamine-induced disruption of 8-arm radial maze performance in rats. Biol. Pharm. Bull. 18, 1439–1442.

Nowakowski, R.S., Lewin, S.B., Miller, M.W., 1989. Bromodeoxyuridine immunohistochemical determination of the lengths of the cell cycle and the DNA-synthetic phase for an anatomically defined population. J. Neurocytol. 18, 311–318.

Packard Jr., D.S., Menzies, R.A., Skalko, R.G., 1973. Incorporation of thymidine and its analogue, bromodeoxyuridine, into embryos and maternal tissues of the mouse. Differentiation 1, 397–404.

Paxinos, G., Watson, C., 1986. The Rat Brain in Stereotaxic Coordinates. Academic Press, San Diego.

Petkov, V.D., Mosharrof, A.H., Petkov, V.V., Kehayov, R.A., 1990. Age-related differences in memory and in the memory effects of nootropic drugs. Acta Physiol. Pharmacol. Bulg. 16, 28–36.

Petkov, V.D., Cao, Y., Todorov, I., Lazarova, M., Getova, D., Stancheva, S., Alova, L., 1992. Behavioral effects of stem-leaves extracts from Panax Ginseng C.A. Meyer. Acta Physiol. Pharmacol. Bulg. 18, 41–48.

Petkov, V.D., Kehayov, R., Belcheva, S., Konstantinova, E., Petkov, V.V., Getova, D., Markovska, V., 1993. Memory effects of standardized extracts of Panax Ginseng (G115) Ginkgo biloba (GK501) and their combination Gincosan (PHL-00701). Planta Med. 59, 106–114.

Saito, H., Tsuchiya, M., Naka, S., Takagi, K., 1977. Effects of Panax Ginseng root on conditioned avoidance response in rats. Jpn. J. Pharmacol. 27, 509–516.

Saito, H., Tsuchiya, M., Naka, S., Takagi, K., 1979. Effects of Panax Ginseng root on acquisition of sound discrimination behavior in rats. Jpn. J. Pharmacol. 29, 319–324.

Salim, K.N., McEwen, B.S., Chao, H.M., 1997. Ginsenoside Rb1 regulates ChAT, NGF and trkA mRNA expression in the rat brain.. Brain Res. Mol. Brain Res. 47, 177–182.

Shan, S.J., Xu, Q.P., Shoyama, Y., 2002. Extract of Yi Zhi Fang improves learning and memory behaviours of mice and its possible mechanisms. Phytother. Res. 5, 449–454.

Silva, A.J., Kogan, J.H., Frankland, P.W., Kida, S., 1998. CREB and memory. Annu. Rev. Neurosci. 21, 127–148.

Vaccarino, F.M., Hayward, M.D., Le, H.N., Hartigan, D.J., Duman, R.S., Nestler, E.J., 1993. Induction of immediate early genes by cyclic AMP in primary cultures of neurons from rat cerebral cortex.. Brain Res. Mol. Brain Res. 19, 76–82.

Wang, B.X., Cui, J.C., Liu, A.J., Wu, S.K., 1983. Studies on the anti-fatigue effect of the saponins of stems and leaves of Panax Ginseng (SSLG). J. Tradit. Chin. Med. 3, 89–94.

Watanabe, H., Ohta, H., Matsumoto, K., 1990. Effect of Ginseng on spontaneous motor activity, water maze learning and central dopaminergic systems in old rats. In: Shibata, S., Ohtsuka, Y., Saito, H. (Eds.), Recent Advances in Ginseng Studies. Tokyo Hirokawa, Tokyo, pp. 73–81.

Wen, T.C., Yoshimura, H., Matsuda, S., Lim, J.H., Sakanaka, M., 1996. Ginseng root prevents learning disability and neuronal loss in gerbils with 5-min forebrain ischemia. Acta Neuropathol. 91, 15–22.

Yoshimura, H., Watanabe, K., Ogawa, N., 1998. Psychotropic effects of Ginseng saponins on agonistic behavior between resident and intruder mice. Eur. J. Pharmacol. 146, 291–297.

Zhao, R., McDaniel, W.F., 1998. Ginseng improves strategic learning by normal and brain-damaged rats. Neuroreport 9, 1619–1624.

Zhong, Y.M., Nishijo, H., Uwano, T., Yamaguchi, H., Ono, T., 1998. Red Ginseng ameliorates place learning deficits in aged rats and in young rats with selective hippocampal lesions. In: Proceedings of the Seventh International Symposium on Ginseng. pp. 1–11.

Cellular/Molecular

Essential Contribution of the Ligand-Binding βB/βC Loop of PDZ1 and PDZ2 in the Regulation of Postsynaptic Clustering, Scaffolding, and Localization of Postsynaptic Density-95

Mio Nonaka,[1,2] Tomoko Doi,[1] Yoshinori Fujiyoshi,[1] Sayaka Takemoto-Kimura,[2] and Haruhiko Bito[2,3]

[1]Department of Biophysics, Kyoto University Graduate School of Science, Kyoto 606-8502, Japan, [2]Department of Neurochemistry, University of Tokyo Graduate School of Medicine, Tokyo 113-0033, Japan, and [3]Solution-Oriented Research for Science and Technology–Japan Science and Technology, Kawaguchi 332-0012, Japan

Postsynaptic density-95 (PSD-95), a PSD-95/Discs large/zona occludens-1 (PDZ) domain-containing scaffold protein, clusters many signaling molecules near NMDA-type glutamate receptors in the postsynaptic densities. Although the synaptic localization of PSD-95 requires palmitoylation of two cysteines at the N terminus and the presence of at least one PDZ domain, how the clustering of PSD-95 is initiated and regulated remains essentially unknown. To address this issue, we examined PSD-95 clustering in primary cultured hippocampal neurons expressing full-length PSD-95 mutant proteins lacking the ligand-binding ability of PDZ1, PDZ2, and/or PDZ3. The formation of either excitatory or inhibitory synapses was unaffected. Combinations of individual mutations, however, significantly reduced the PSD-95 clustering index, in an approximately additive manner. The sensitivity to 2-bromo-palmitate and latrunculin A, reagents known to affect PSD-95 turnover, was also augmented. Furthermore, the synaptic recruitment of a PSD-95 ligand, synaptic GTPase-activating protein (synGAP), was significantly impaired, whereas the clustering of other scaffolding proteins, such as Homer 1c, Shank/Synamon, and PSD-93/Chapsin-110 was spared. Intriguingly, overexpression of the PSD-95 PDZ1/2/3 mutants caused the PSD-95 clusters to localize away from the dendritic shaft, resulting in the formation of elongated spines, in an inverse correlation with the overall PDZ-ligand affinity. Expression of a mutant synGAP lacking the PDZ-binding motif replicated both the clustering and spine morphology phenotypes. In conclusion, the ligand-binding affinity of the PDZ domains of PSD-95, contributed in part via its interaction with the C-terminal end of synGAP, plays a critical role in titrating the synaptic clustering of PSD-95 and controlling its tight association with the PSD scaffold, thereby affecting synapse maturation.

Key words: PSD-95; clustering; spine; synGAP; NMDA receptor; PDZ domains; binding affinity

Introduction

The postsynaptic density (PSD) is an electron-dense structure in which neurotransmitter receptors and associated signaling molecules are tightly clustered. This postsynaptic receptor complex plays an essential role in converting bouts of neurotransmitter release at chemical synapses into postsynaptic electrical and chemical signaling. Knock-in mice expressing a mutant NMDA-type glutamate receptor (NR) subunit 2B, lacking the intracellular C-terminal domain, displayed deficient synaptic properties reminiscent of NR1 knock-out mice (Sprengel and Single, 1999). Therefore, a physical link between the NMDA receptor and the downstream signaling and/or scaffolding molecules appears crucial for establishing normal synaptic function.

A major scaffold protein interacting with the NMDA receptor is PSD-95. This membrane-associated guanylate kinase (MAGUK) superfamily member possesses three N-terminal PSD-95/Discs large/zona occludens-1 (PDZ) domains, a central Src homology 3 (SH3) domain, and a C-terminal guanylate kinase (GK)-like domain (Cho et al., 1992; Kim et al., 1995; Kornau et al., 1995). Different ligand proteins interact with these three class I PDZ domains with various specificities and affinities (Sheng and Sala, 2001). For instance, synGAP (synaptic GTPase-activating protein) (Chen et al., 1998; Kim et al., 1998) binds to each PDZ equally. In contrast, the C-terminal PDZ-binding motif (–ESDV) of the NR2 subunit binds to PDZ1 and PDZ2 (Kornau et al., 1995), whereas ligands such as neuroligin (Irie et al., 1997) and cysteine-rich interactor of PDZ3 (CRIPT) (Niethammer et al., 1998) preferentially interact with PDZ3.

Extensive deletion mutagenesis studies established that the clustering of PSD-95 involves multimerization mediated by the

Received June 17, 2005; revised Nov. 18, 2005; accepted Nov. 22, 2005.

This work was supported by grants-in-aid from the Ministry of Education, Culture, Sports, Science, and Technology of Japan (Y.F., H.B.) and by grants from the Human Frontier Science Program, Solution-Oriented Research for Science and Technology–Japan Science and Technology, and the Ministry of Health, Labor, and Welfare of Japan (H.B.). We thank Dr. Yutaka Hata (Tokyo Medical and Dental University, Tokyo, Japan) for providing the Shank antibody, Dr. Hideru Togashi (Center for Developmental Biology, RIKEN, Kobe, Japan) for assistance with low-density rat primary culture and electroporation techniques, and Dr. Toshifumi Tomoda (City of Hope National Medical Center, Beckman Research Institute, Duarte, CA) and Dr. Richard L. Huganir (Johns Hopkins University, Baltimore, MD) for the synGAP cDNAs. We also thank Dr. Makoto Goda for assistance with the light microscopy systems, Ayako Tanaka for cloning the CRIPT cDNA, Taichi Okamoto for technical assistance, and Dr. Hiroyuki Okuno for discussions on statistical data analysis.

Correspondence should be addressed to Tomoko Doi, Department of Biophysics, Kyoto University Graduate School of Science, Kitashirakawa-oiwake, Sakyo, Kyoto 606-8502, Japan. E-mail: doi@em.biophys.kyoto-u.ac.jp.

DOI:10.1523/JNEUROSCI.2489-05.2006

Copyright © 2006 Society for Neuroscience 0270-6474/06/260763-12$15.00/0

N-terminal region containing palmitoylated Cys-3 and Cys-5, and that the presence of one PDZ domain is sufficient for its synaptic targeting (Craven et al., 1999; Hsueh and Sheng, 1999; Christopherson et al., 2003). The importance of the tandem order of PDZ domains and of the short linker between them has also been suggested (Long et al., 2003). Furthermore, the PDZ-ligand interactions probably trigger and promote clustering via intermolecular interactions through the SH3–GK domains (Brenman et al., 1998; McGee et al., 2001; Tavares et al., 2001). However, the individual contribution of each PDZ domain and the impact of the series of ligand-binding sites on the clustering and scaffolding functions of PSD-95 have not been quantitatively examined.

To address these questions, we used PSD-95 mutants with an intact overall protein length and domain structure, in which specific mutations were introduced at the ligand-binding βB/βC loop of the PDZ1 and/or PDZ2 domains (Imamura et al., 2002). These PDZ1/2 ligand-binding site mutants were further combined with the N326S mutation in PDZ3, which greatly reduces the PDZ3–ligand affinity (Niethammer et al., 1998). By overexpressing these PSD-95 mutants with either individual or combined PDZ mutations in cultured hippocampal neurons, we probed the contributions of the individual ligand-binding sites in the clustering, membrane anchoring, and scaffolding functions of PSD-95. Our results suggested that multivalent ligand binding via the βB/βC loops of PDZ1 and PDZ2, in part by interacting with synGAP, not only plays a critical role in titrating the synaptic clustering and anchoring of PSD-95 but also, surprisingly, contributes to attracting the PSD-95-based scaffold to the proximity of dendritic shafts during synapse maturation.

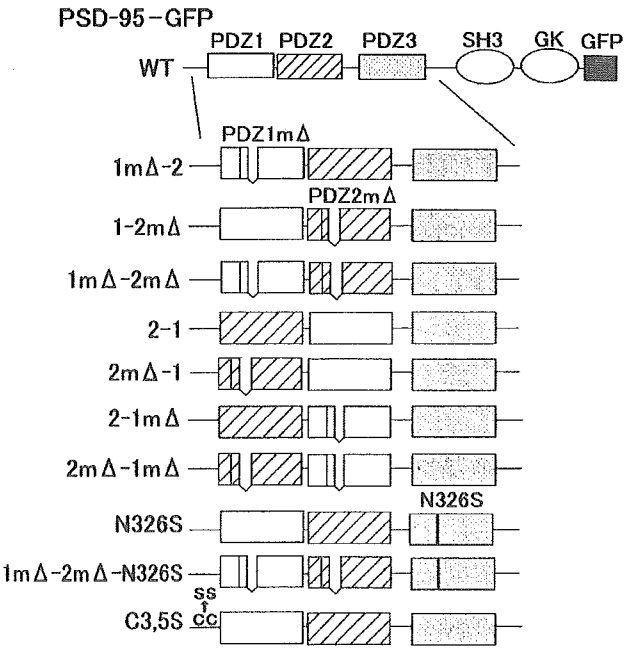

Figure 1. Schematic diagram of the domain structures of the series of PSD-95–GFP mutants and the wild type. The top panel shows the domain structure of PSD-95 tagged with GFP at the C terminus. The mutant illustrations show the N-terminal segment of PSD-95, including only the PDZ domains. PDZ1mΔ and PDZ2mΔ represent the PDZ1 and PDZ2 domains, respectively, with deletions of six amino acids (intervals) and point mutations that abolished their ligand-binding activity. The PDZ3 domain with the N326S point mutation (black vertical bar) has weak ligand-binding activity.

Materials and Methods

DNA constructs. The mutated PSD-95 cDNAs were constructed as described previously (Imamura et al., 2002). These were fused to enhanced green fluorescent protein (EGFP) via a linker sequence, Gly-Gly-Gly-Ser, using PCR in the EGFP-N1 vector (BD Biosciences-Clontech, Palo Alto, CA). The C3,5S and N326S mutations were introduced using a Quikchange mutagenesis kit (Stratagene, La Jolla, CA). The pRK5-synGAP(TRV) cDNA tagged with N-terminal Myc was obtained from Toshifumi Tomoda (City of Hope National Medical Center, Beckman Research Institute, Duarte, CA) with permission from Richard Huganir (Johns Hopkins University, Baltimore, MD), and mutagenesis was performed by PCR. All constructs were confirmed by DNA sequencing.

Primary culture, transfection, and immunocytochemistry. For immunocytochemical analyses, we prepared primary cultures of hippocampal neurons from either ICR mice or Wister rats, purchased from Japan SLC (Shizuoka, Japan). The high-density primary culture from postnatal days 0 to 1 mouse hippocampus was performed as described previously (Furuyashiki et al., 2002). Briefly, 4×10^4 cells were plated onto Matrigel (BD Biosciences, Bedford, MA)-coated spots of ~5 mm in diameter on glass coverslips, and the cultured neurons were fed with fetal calf serum-containing medium in the presence of Ara-C (Sigma, St. Louis, MO). Cultured neurons were transfected at 9 d *in vitro* (DIV) using the calcium phosphate method (Takemoto-Kimura et al., 2003), and then the cells were fixed at 12 DIV. In cotransfection experiments examining the effect of overexpressing wild-type (WT) or mutant synGAP, neurons were transfected at 8 DIV by lipofection using Lipofectamine 2000 (Invitrogen, Carlsbad, CA), and cell phenotypes were examined at 10 DIV.

For immunocytochemistry, neurons were fixed in PBS(−) containing 4% paraformaldehyde/4% sucrose (or 2% paraformaldehyde/4% sucrose for PSD-93 staining). Fixed neurons were quenched in 0.1 M glycine/PBS(−), permeabilized with 0.2% Triton X-100/PBS for 10 min on ice, thoroughly washed with PBS(−), incubated in blocking solution [3% BSA/PBS(−)] for 30 min at room temperature, and then incubated overnight with primary antibodies (listed below) diluted in the blocking buffer at 4°C. The next day, the neurons were washed three times with PBS(−) and then were incubated with Alexa Fluor-conjugated secondary antibodies (Invitrogen) at a 1:500 dilution in blocking buffer. The antibody sources and dilutions are as follows: rabbit polyclonal anti-vesicular glutamate transporter-1 (VGLUT1) (1:1000; Synaptic Systems, Goettingen, Germany), monoclonal anti-vesicular GABA transporter (VGAT) (1:1000; Synaptic Systems), monoclonal anti-synaptophysin (1:1000; Sigma), monoclonal anti-PSD-95 [K28/43, 1:200 (Upstate Biotechnology, Lake Placid, NY); 7E3–1B8, 1:250 (Affinity BioReagents, Golden, CO)], monoclonal anti-synGAP (1:1000; Affinity BioReagents), rabbit polyclonal anti-Homer-1c (Irie et al., 2002), rabbit polyclonal anti-PSD-93 (1:250; Zymed, San Francisco, CA), rabbit polyclonal anti-Synamon/Shank (a kind gift from Yutaka Hata, Tokyo Medical and Dental University, Bunkyo-ku, Tokyo, Japan), polyclonal anti-Myc (1:200; Cell Signaling Technology, Beverly, MA), and Alexa Fluor-conjugated anti-rabbit and anti-mouse antibodies (1:500; Invitrogen).

Pharmacological treatments. Pharmacological treatments were performed by low-density rat hippocampal cultures, and the resulting effects were examined by immunofluorescent (IF) staining, as described previously (Togashi et al., 2002). The PSD-95 mutant phenotypes reported in this study were essentially identical, regardless of the type of primary culture (data not shown). At 12 or 13 DIV, one-half of the culture medium was removed from the dish, and 2-bromo-palmitate (2-Br-Pal) or latrunculin A (LatA) (from a 1000× stock in DMSO) were mixed with this half, to concentrations of 200 and 10 μM, respectively. This medium was then returned to the culture dish and mixed well with the remaining medium by gentle rocking. After either a 2 or 8 h treatment, the cells were washed with cold PBS(−) and fixed immediately. Latrunculin A was obtained from Calbiochem (La Jolla, CA), and 2-Br-Pal (2-bromohexadecanoic acid) was from Sigma.

Quantitative microscopy and image analysis. All immunofluorescence images were acquired using a cooled CCD camera (Orca II; Hamamatsu Photonics, Hamamatsu, Shizuoka, Japan), controlled by the MetaVue or MetaMorph software (Molecular Devices, Sunnyvale, CA) and mounted on either a BX50 upright or an IX-81 inverted microscope (Olympus Optical, Tokyo, Japan) with 100× [numerical aperture (NA), 1.35] and

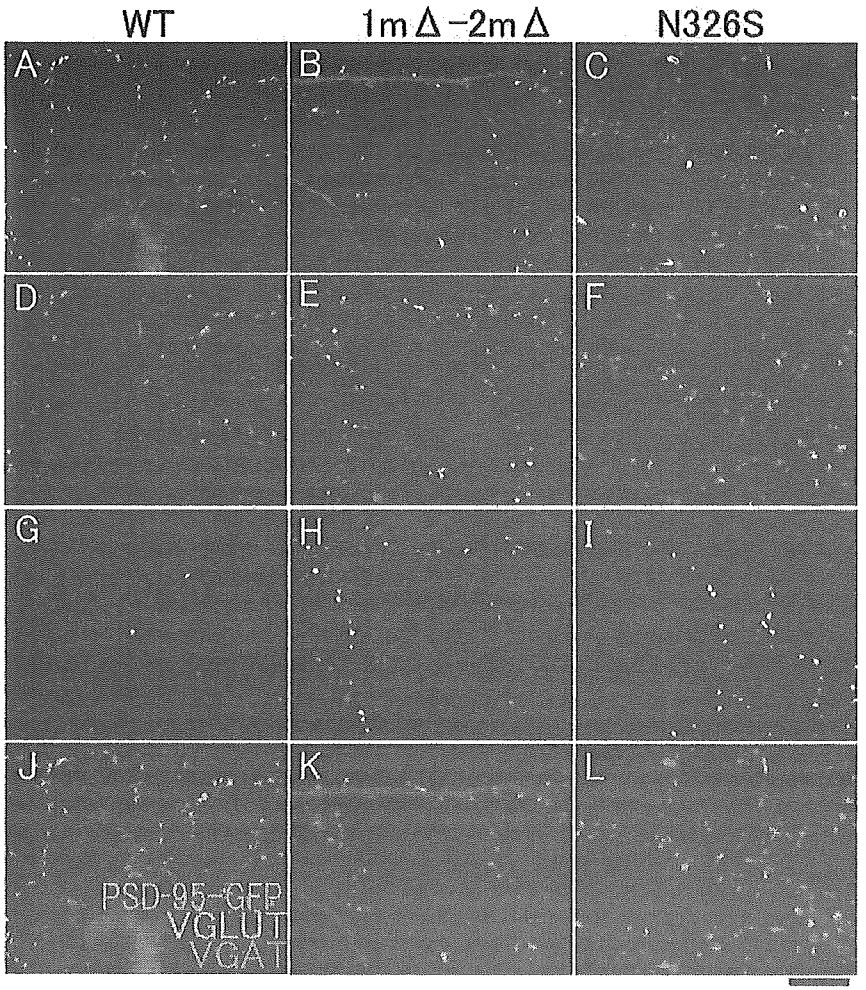

Figure 2. Wild-type and mutant PSD-95 form postsynaptic clusters apposed to the glutamatergic synaptic boutons. The PSD-95(WT)–GFP, 1mΔ-2mΔ, and N326S (***A–C*** and green in ***J–L***, respectively) form clusters juxtaposed to puncta immunopositive for an excitatory presynaptic marker, anti-VGLUT1 (***D–F*** and red in ***J–L***). No cluster colocalized with puncta positive for an inhibitory presynaptic marker, anti-VGAT (***G–I*** and blue in ***J–L***). The bottom images are merged images in which PSD-95–GFP staining is green, VGLUT1 staining is red, and VGAT staining is blue. Scale bar, 10 μm.

40× (NA, 0.85) objectives and filter cubes appropriate for costaining of GFP, Alexa 594, and Alexa 350, or GFP, Alexa 555, and Alexa 647. Immunostaining and image acquisition were performed using rigorously identical procedures within a set of experiments, which enabled us to obtain reproducible sets of immunofluorescence values, as detected by the cooled CCD camera.

For quantification purposes, only the neurons that expressed PSD-95–GFP within the average intensity values of 100–300 (in a 12-bit dynamics range, 0–4096 at a fixed gain setting) in the dendritic shafts were considered and randomly chosen, because most of the cells with normal morphology fell within this value range. In the preliminary series of experiments, the minimum and maximum intensity values, 100 and 300, were set as reliable thresholds to obtain a sufficient amount of mutant proteins to reveal a dominant phenotype and to avoid the toxic effects attributable to the overexpression of exogenous proteins, respectively. For each cell, one to four images were acquired to cover the main dendritic area. The dendritic segments (the apparent dendritic shaft diameter was >0.7 μm) were chosen randomly within 200 μm from the soma. For the synaptic clustering index (SCI), cluster density (the number of clusters per 20 μm dendritic segment), and cluster-shaft distance measurements, the PSD-95 clusters were defined as 0.3–1.0 μm diameter spots of increased GFP fluorescence, at least twice as bright as the dendritic shaft (to discriminate true clusters from stochastic local gradients; however, because of spatial resolution limitations, we were unable to reliably resolve clusters less than ~0.2 μm in diameter), which were closely juxtaposed to synaptophysin-immunopositive puncta. In the obtained ensemble dataset, both the cluster size and average cluster fluorescence intensity followed a Gaussian distribution, indicating that no systematic bias was introduced by these criteria.

The SCI was calculated off-line with the MetaVue or MetaMorph software, essentially as described previously (Arnold and Clapham, 1999), using images acquired with the 100× (NA, 1.35) objective. Briefly, after subtracting the background, the maximal intensity of each synaptic cluster was divided by the average intensity of the proximal parent dendritic shaft. The average dendritic shaft intensity was measured by drawing an orthogonal line traversing the dendritic area immediately nearest/adjacent to the cluster but excluding any outlying bright spots. Because we used wide-field microscopy, the inclusion of immunofluorescence values obtained from out-of-focus fields would inevitably result in underestimation and inexact SCI values. To avoid this, we determined the in-focus area of interest within each image and only analyzed the immunofluorescence values obtained from dendrites and clusters located within that area. In control experiments, the SCI analysis performed over the same fields of view, using a 40× objective lens, yielded quantitatively similar results, confirming that under our experimental conditions, the contribution of the out-of-focus photons was negligible, even with the 100× (NA, 1.35) objective (data not shown).

For the cluster-shaft distance measurement, the images were displayed at the same magnification, and the synaptic clusters were chosen using the same criteria as for the SCI measurement. A line was manually drawn off-line from the center of each synaptic cluster to the nearest edge of their parent dendritic shafts, and the length was measured using the MetaVue or MetaMorph software. A distance value of zero was applied to those clusters formed directly on the dendritic shaft (shaft clusters). We acknowledge the caveat that such data obtained from projection images strongly underestimate the protrusion into the *z*-axis but this does not alter the main results of our analyses, because this *z*-axis underestimation factor is equally distributed across the *x*–*y* plane, although the correlation factor obtained in Figure 7*A* may be slightly underrepresented.

The SCI and cluster-shaft distance values were thus calculated for 20–100 clusters from at least 100 μm of dendritic segments per cell, and the average values for each cell were further subjected to a multicomparison analysis. Six to 11 cells were analyzed in total for each individual PSD-95 mutant construct. For the statistical analysis, the SCI measurement was evaluated by one-way ANOVA, with the *post hoc* Dunnett's test, using the JMP software (SAS Institute, Toronto, Ontario, Canada), and the cumulative distribution of the cluster-shaft distances was analyzed by the Kolmogorov–Smirnov test, using the PAST software (Hammer et al., 2001). Graphs were made with the Prism software (GraphPad Software, San Diego, CA) and Excel (Microsoft, Seattle, WA).

Results

Construction of full-length PSD-95 mutants containing PDZ domains with reduced binding affinity

The mutant PDZ domains, PDZ1mΔ and PDZ2mΔ, in which the ligand-binding βB/βC loop of either the PDZ1 or PDZ2 domain

of PSD-95 was altered, were shown previously to be unable to bind to NR2B and Kv1.4, both *in vitro* and in a heterologous system (Imamura et al., 2002). We further confirmed that they are also unable to bind CRIPT, a well known neuronal PDZ3 ligand, despite the apparent homology between the mutated PDZ1/2 sequences and PDZ3 (supplemental Fig. 1, available at www.jneurosci.org as supplemental material). To further disrupt the ligand binding at the PDZ3 domain, we introduced an additional point mutation, N326S (Niethammer et al., 1998). This significantly reduced the binding of mutated PDZ3 to CRIPT and allowed only weak binding to Kv1.4 (supplemental Fig. 1, available at www.jneurosci.org as supplemental material). Based on these results, we next systematically replaced the PDZ1, PDZ2, and PDZ3 of PSD-95 with PDZ1mΔ, PDZ2mΔ, and PDZ3 (N326S) and fused EGFP at their respective C termini. Figure 1 shows the series of PSD-95–GFP mutants used in this study. The PDZ1–PDZ2 inverted mutants were also constructed to test whether the relative positions of the PDZ domains were as important in cultured neurons as in a heterologous expression system (Imamura et al., 2002).

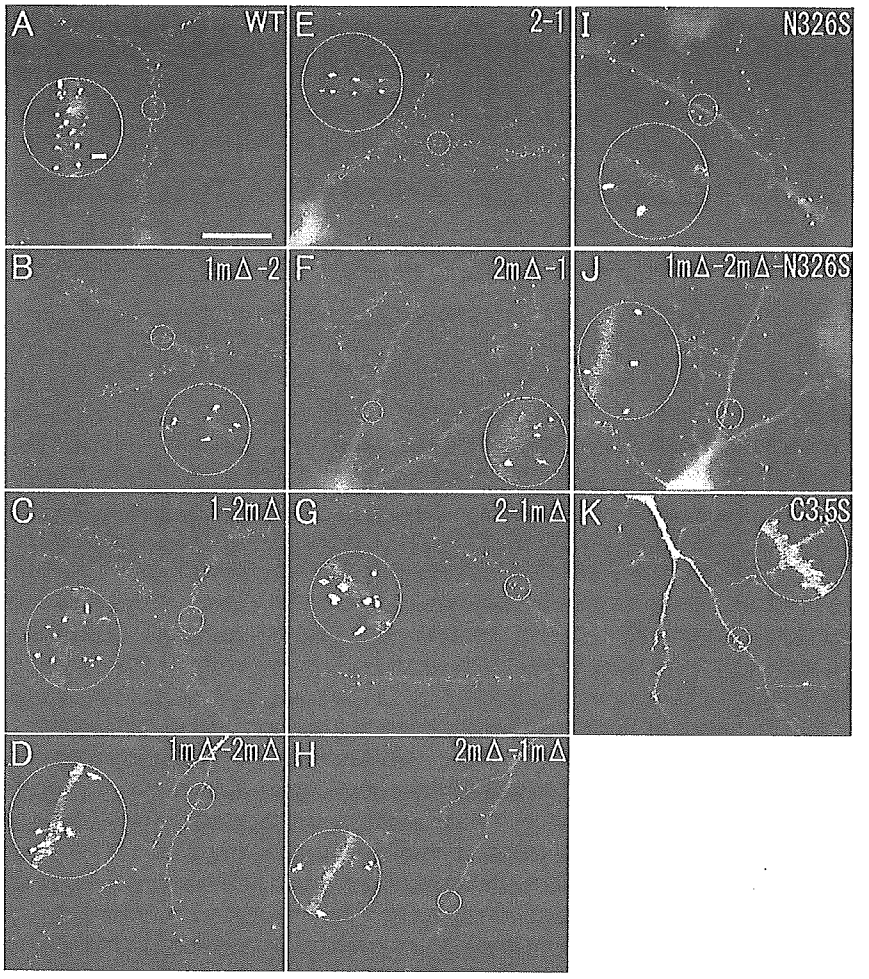

Figure 3. Synaptic clustering of PSD-95 is diminished by PDZ-ligand-binding mutations. GFP fluorescent images were taken from transfected hippocampal neurons expressing the wild-type (***A***) and the series of mutant PSD-95–GFPs (***B–K***). ***A***, ***E***, The wild-type and the 2–1 (inversion of PDZ1 and PDZ2, with intact ligand-binding affinity) mutant formed bright shaft clusters. Note that the majority of the clusters are shaft clusters. ***B***, ***C***, ***F***, ***G***, When either the PDZ1 or PDZ2 domain is mutated, the clustering activity is slightly reduced. A significant number of clusters are formed at some distance from the dendritic shaft, indicating their presence on spine-like protrusions. ***D***, ***H***, Mutations in both PDZ1 and PDZ2 reveal clusters located farther away, on the tips of longer protrusions. In contrast to the WT, the fluorescence intensity of these clusters is not substantially higher compared with the mean dendritic shaft intensity. ***I***, The N326S mutation in the PDZ3 domain also reduces the clustering efficiency. ***J***, 1mΔ–2mΔ–N326S, the mutant that lacks functional PDZ domains, forms discernible clusters juxtaposed to the presynaptic markers, but the clustering efficiency is extremely low. The clusters are even farther from their parent dendritic shafts. All of the ligand-binding-deficient mutants are distinct from the C3,5S mutant (***K***) in that they form punctate clusters. Scale bars: 20 μm; inset, 1 μm. The insets are the magnified images of the areas outlined by white circles in the images. All of the insets have the same magnification.

Individual PDZ domains independently and additively contribute to the synaptic clustering of PSD-95

To examine the role of ligand binding to each individual PDZ domain in postsynaptic clustering during synaptic maturation, we transfected the cDNAs for each PSD-95–GFP mutant in cultured mouse hippocampal neurons at 9 DIV. Neurons were fixed at 12 DIV and immunostained with a presynaptic marker. We first confirmed that exogenous PSD-95(WT)–GFP and PSD-95(1mΔ–2mΔ)–GFP formed clusters in puncta of ~0.3–0.4 μm in diameter. These PSD clusters were juxtaposed to puncta immunoreactive to VGLUT1, a marker for excitatory glutamatergic termini, but were far from puncta immunoreactive to VGAT, a marker for inhibitory GABAergic termini (Fig. 2). We initially calibrated the expression levels of the PSD-95–GFP constructs by comparing the anti-PSD-95-immunoreactive signals of untransfected neurons with those of transfected neurons containing both exogenous and endogenous PSD-95. We established that, at a fixed gain setting, using our cooled CCD acquisition system, neurons with mean GFP intensities in dendritic shafts between 100 and 300 had a dendritic morphology indistinguishable from that of untransfected neurons. The anti-PSD-95 immunoreactivity completely overlapped with the GFP puncta, and the GFP fluorescence intensities of 100–300 corresponded to ~3.4- to 5.6-fold higher amounts of PSD-95 immunoreactivity compared with the basal, endogenous levels in untransfected cells. In the mutant PSD-95–GFP containing PDZ1mΔ, the distribution of endogenous PSD-95, stained using a PSD-95 antibody (7E3–1B8) that did not recognize the PDZ1mΔ, was indistinguishable from the GFP fluorescence from the mutant PSD-95 molecules (data not shown). Furthermore, we confirmed that the overexpression of the full-length wild-type or mutant PSD-95–GFP constructs in neurons apparently had minimal effects on the integrity of the full-length protein (supplemental Fig. 2, available at www.jneurosci.org as supplemental material). The wild-type and mutant PSD-95–GFP were able to form complexes when expressed in COS cells, because they coimmunoprecipitated together (data not shown). Thus, the exogenously expressed PSD-95–GFP freely intermingled with the endogenous PSD-95. Therefore, any phenotypic change resulting from overexpressing the mutant PSD-95, as opposed to overexpressing the wild-type PSD-95, was likely to result from a dominant effect triggered by the reduced binding affinity of the mutated PDZ domain(s).

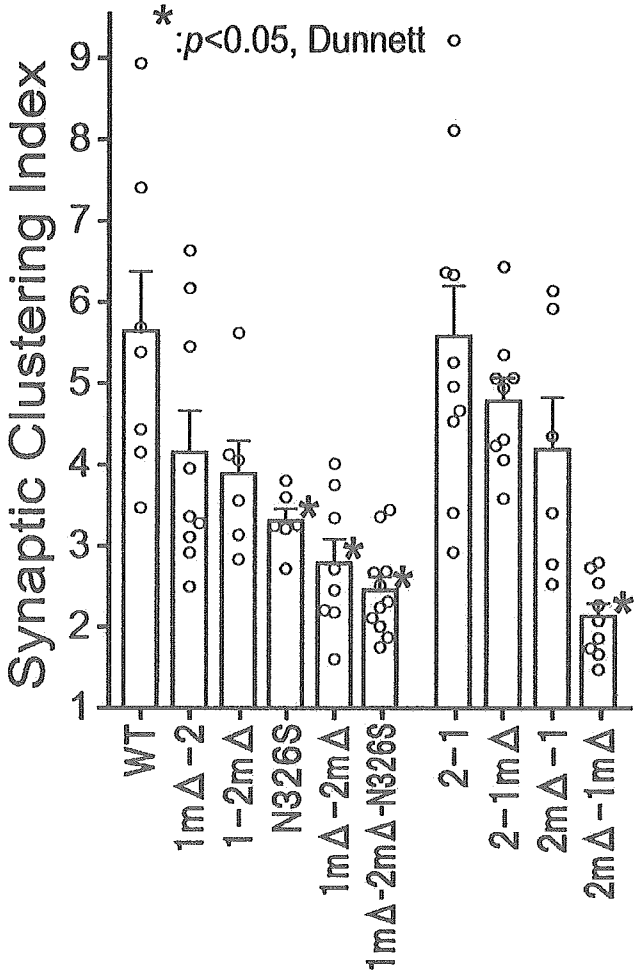

Figure 4. Individual PDZ domains independently and additively contribute to postsynaptic clustering of PSD-95. The SCI was measured as the peak GFP intensity of the synaptic PSD-95–GFP clusters divided by the average intensity of the parent dendritic shaft. Wild-type PSD-95 forms clusters that are 5.64 ± 0.73 times as bright as the parent dendritic shaft, on average. In contrast, the 1mΔ–2mΔ mutant forms clusters with an SCI of approximately half of the wild type (SCI, 2.79 ± 0.298; $p < 0.05$ vs WT). Open bars and error bars are means ± SEM of the cell averages ($n = 6–11$ cells), and open circles represent the average of each cell (20–100 clusters per cell). We confirmed that the SCI values of each cluster in a cell conformed to a normal distribution. Each dataset was statistically analyzed by one-way ANOVA, with the *post hoc* Dunnett's test. *$p < 0.05$ versus WT.

To quantitatively measure the clustering efficiency at the postsynaptic site, we used the SCI (Arnold and Clapham, 1999). Basically, the SCI was calculated as the peak GFP pixel intensity at the clusters juxtaposed to the presynaptic markers divided by the average GFP pixel intensity of the adjacent dendritic shaft (see Materials and Methods). The SCI value varied from cluster to cluster and cell to cell, but the values exhibited a normal distribution (data not shown). The average SCI of the wild type was 5.64 ± 0.73 (mean ± SEM) (Figs. 3*A*, 4). The C3,5S mutant, which lacks the two palmitoylation sites at the N terminus, was localized diffusely (Fig. 3*K*), as reported previously (Craven et al., 1999). In contrast to the C3,5S mutant, all of the ligand-binding-deficient mutants formed distinguishable clusters (Fig. 3*B–J*) juxtaposed to the presynaptic marker synaptophysin. However, the synaptic clusters of these mutants were less dense, with a substantial portion of the PSD-95–GFP molecules remaining unclustered in dendritic shafts (Fig. 3*D*,*H*,*J*). Noticeable degradation of the PSD-95–GFP proteins in transfected neurons overexpressing either the wild-type or mutant PSD-95–GFP proteins was not detected (supplemental Fig. 2, available at www.jneurosci.org as supplemental material), indicating that the loss of synaptic clustering probably resulted from dispersion rather than protein degradation. The postsynaptic clustering activity was significantly attenuated in the 1mΔ–2mΔ mutant compared with the wild type (Fig. 4) (SCI, 2.79 ± 0.30; $p < 0.05$, ANOVA with the *post hoc* Dunnett's test). The N326S mutation in PDZ3 also significantly reduced the clustering efficiency (SCI, 3.18 ± 1.87; $p < 0.05$, ANOVA with the *post hoc* Dunnett's test), to an extent approximately comparable with that of the 1mΔ–2mΔ mutant. These results suggested that synaptic clustering is not only governed by ligand binding to the PDZ3 domain, whose contribution was shown previously in a peptide inhibition experiment (Passafaro et al., 1999), but also by ligand binding to both PDZ1 and PDZ2. Consistent with this idea, the 1mΔ–2mΔ–N326S mutant exhibited the lowest clustering efficiency of all of the non-inverted mutants (SCI, 2.44). The inversion of the mutated PDZ domains had no discernable effect per se on synaptic clustering in hippocampal neurons ($SCI_{2mΔ-1}$, 4.19 ± 0.64, $SCI_{2-1mΔ}$, 4.78 ± 0.28 vs $SCI_{1mΔ-2}$, 4.15 ± 0.51, $SCI_{1-2mΔ}$, 3.89 ± 0.40), unlike the results seen previously in a heterologous expression system with only Kv1.4 as a ligand (Imamura et al., 2002). This probably reflects the complexity of the stoichiometry and the competition among multiple PDZ ligands for PSD-95 binding within the small volume of the PSD near physiological synapses.

Collectively, these observations support the notion that the ligand binding to PDZ1, PDZ2, and PDZ3 independently contributes to the postsynaptic clustering of PSD-95 at the PSD, and that this regulation operates in an approximately additive manner.

Postsynaptic clustering of a PSD-95 ligand, synGAP, is severely altered in PSD-95 mutant expressing neurons, but the clustering of Shank/Synamon, Homer, and PSD-93 remains intact

We next tested whether a loss in PDZ binding affinity in PSD-95 affected the recruitment of a nontransmembrane PDZ ligand or PSD scaffolds distinct from PSD-95 by performing immunocytochemical analyses in synaptic clusters of wild-type and mutant expressing neurons. We found no significant difference in the immunoreactivity (IF) intensity at synaptic clusters for either Shank/Synamon, Homer 1c/Vesl-L/PSD-Zip45, or PSD-93/Chapsin-110, three postsynaptic molecular scaffold proteins distinct from PSD-95, between the neurons expressing wild-type PSD-95 and the 1mΔ–2mΔ mutant ($p > 0.5$ in all IF experiments) (Fig. 5*C–E*). In contrast, the staining intensity for synGAP, a major PSD-95 ligand, was significantly reduced in the neurons expressing the 1mΔ–2mΔ and 1mΔ–2mΔ–N326S PSD-95 mutants compared with the wild-type expressing neurons (Fig. 5*A*,*B1*,*B2*) [mean ± SEM; WT, 2.88 ± 0.20; 1mΔ–2mΔ, 1.9 ± 0.17; $p < 0.05$ (*t* test) vs WT; and WT, 3.4 ± 0.62; 1mΔ–2mΔ–N326S, 1.7 ± 0.12; $p < 0.05$ (*t* test) vs WT]. These results suggest that the impact of the reduced PDZ-ligand affinity of PSD-95 is limited to the primary PSD-95 ligands and may not extend to other PSD proteins indirectly associated with PSD-95 via the scaffolding complexes present in the PSD.

Loss of the ligand-binding affinity in PDZ domains destabilizes the PSD-95 association with the PSD

Previous work examining PSD-95 turnover at and near synapses demonstrated that only a limited pool of PSD-95 undergoes active turnover (Okabe et al., 1999), and an EM study further suggested that PSD-95 is deeply anchored to the core fraction (<12 nm from the postsynaptic membrane) of the PSD (Petersen et al., 2003). To investigate whether the PDZ-ligand binding plays a role in the tight integration of PSD-95 in the PSD, we treated neurons with 100 μM 2-bromo-palmitate, a reagent that blocks palmitoylation (El-Husseini Ael et al., 2002) and thereby inhibits the delivery of PSD-95 to plasma membranes. Within 2 h after treatment, the synaptic clustering of PSD-95 in the wild-type expressing neurons, measured using SCI, only decreased by 14.2% compared with the vehicle-treated control, whereas the SCI in the mutant (1mΔ–2mΔ) PSD-95 expressing neurons significantly decreased to almost half of that of the control (55.7%; $p < 0.01$, Student's t test) (Fig. 6*A*). After an 8 h incubation, the SCI values of the wild-type expressing neurons were reduced to a level similar to that of the 1mΔ–2mΔ mutant. Thus, the removal of PSD-95 from the synaptic clusters was facilitated in the 1mΔ–2mΔ mutant as a result of the reduced delivery of new palmitoylated PSD-95 to the surface membranes. This result suggests that intact PDZ1/2 ligand binding may contribute to synaptic clustering by either promoting the aggregation of palmitoylated PSD-95 molecules or facilitating the maintenance of the palmitoylated form of PSD-95.

We then tested the PSD-95 mutants for a potential alteration in the susceptibility of postsynaptic clustering to 5 μM LatA, a reagent that favors filamentous actin (F-actin) depolymerization within spines (Allison et al., 1998). In the wild-type PSD-95 expressing neurons, LatA treatment for 17 h was required to substantially reduce the SCI. Even after 17 h of treatment, distinct clusters remained on dendrites ($SCI_{0\ h}$, 6.31 ± 0.30; $SCI_{17\ h}$, 4.12 ± 0.20; $p < 0.01$) (Fig. 6*B*). In contrast, in the 1mΔ–2mΔ mutant expressing neurons, the clusters readily dissociated within 1.5 h ($SCI_{0\ h}$, 3.63 ± 0.086; $SCI_{1.5\ h}$, 2.61 ± 0.23; $p < 0.01$). However, when scaled to the untreated cells, the SCI values of the wild-type and 1mΔ–2mΔ expressing neurons both decreased, to 65.3 and 61.8% of the original levels, respectively, after 17 h of treatment. Therefore, similar to the

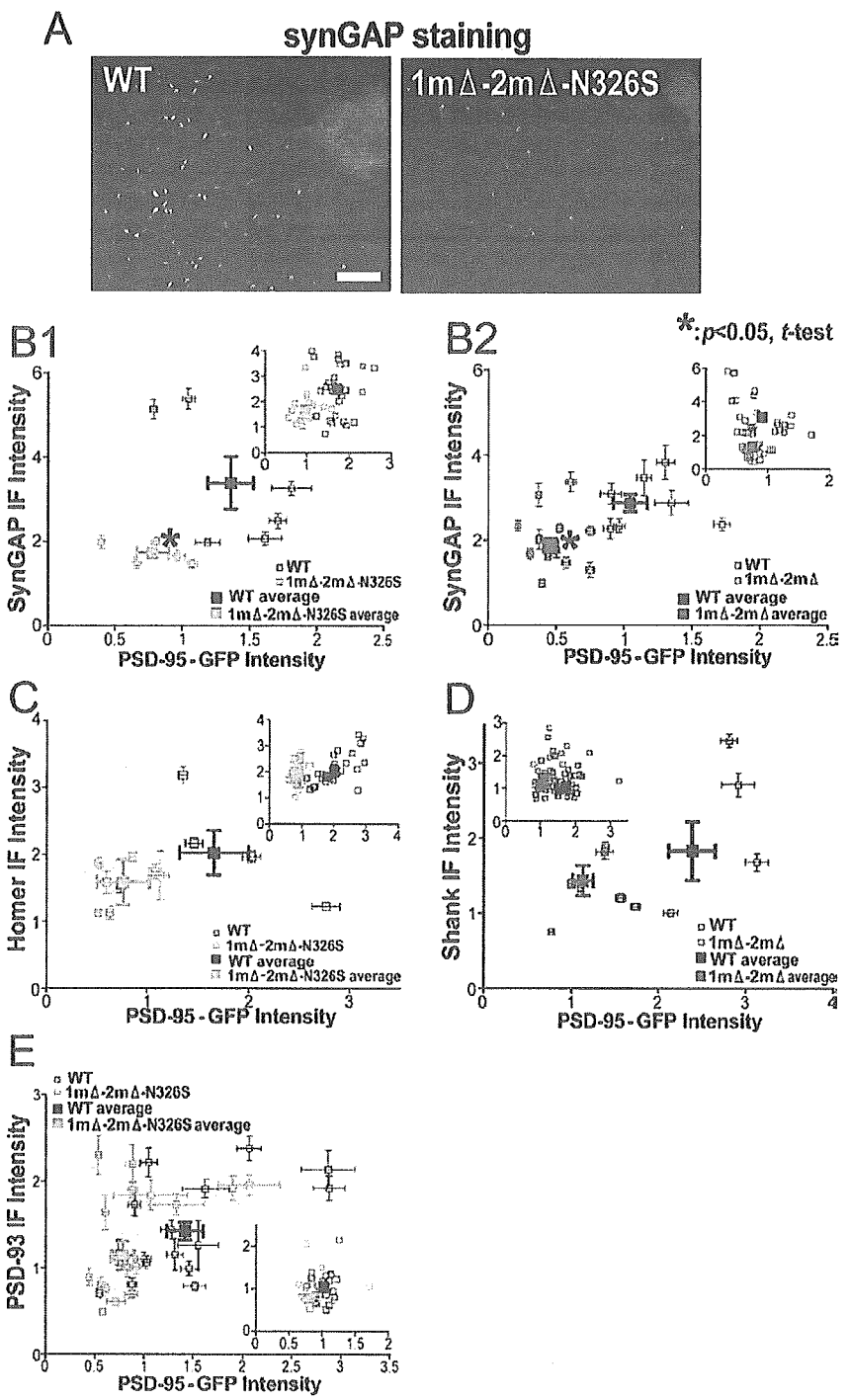

Figure 5. SynGAP immunoreactivity is significantly reduced in the postsynaptic clusters of 1mΔ–2mΔ PSD-95-expressing neurons compared with the wild-type PSD-95-expressing neurons. ***A***, SynGAP IF images of the cells expressing PSD-95(WT)–GFP and 1mΔ–2mΔ–N326S are shown in grayscale. The staining signal is significantly reduced in the postsynaptic clusters of the 1mΔ–2mΔ PSD-95-expressing neurons compared with the wild-type PSD-95-expressing neurons. Scale bar, 10 μm. ***B–E***, Graphs represent the plots of the IF intensities of synGAP (***B***), Homer (***C***), Shank (***D***), and PSD-93 (***E***) versus the PSD-95–GFP intensities of the clusters in the neurons expressing wild-type or mutant PSD-95–GFP (black open squares, wild type; blue open squares, 1mΔ–2mΔ mutant; red open squares, 1mΔ–2mΔ–N326S mutant; filled squares, their averages). Insets are the plots of each cluster observed in one representative neuron. In the main graphs, each small square with bars indicates the averaged value ± SEM of each neuron [GFP intensity to the x-axis (arbitrary units) and IF intensity to the y-axis (arbitrary units)]. All of the cells analyzed expressed approximately similar amounts of PSD-95–GFP in the dendritic shaft, regardless of the mutant type. Therefore, the PSD-95–GFP intensities reflect the SCI values. ***B***, The IF intensities of a major PSD-95 ligand, synGAP, are significantly lower in the 1mΔ–2mΔ–N326S clusters (***B1***, red) and the 1mΔ–2mΔ clusters (***B2***, blue) compared with the PSD-95(WT)–GFP clusters (black). ***C–E***, In contrast, using the same assay, the IF intensities for other scaffold proteins distinct from PSD-95, such as Homer-1c (***C***), Shank/Synamon (***D***), and PSD-93/Chapsin-110 (***E***), are not significantly altered in the postsynaptic clusters ($p > 0.5$). *$p < 0.05$ versus WT by Student's t test.